Estimation of Motion and Depth from Smeared Images

by

Rajiv Kumar Bajpai

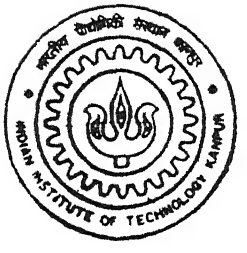

DEPARTMENT OF ELECTRICAL ENGINEERING

INDIAN INSTITUTE OF TECHNOLOGY, KANPUR

February, 2001

Estimation of Motion and Depth from Smeared Images

A Thesis Submitted
in Partial Fulfillment of the Requirements
for the Degree of
Master of Technology

by
Rajiv Kumar Bajpai

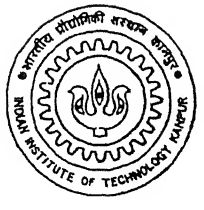

to the
Department of Electrical Engineering
Indian Institute of Technology, Kanpur

February, 2001

Certificate

This is to certify that the work contained in the thesis entitled "*Estimation of Motion and Depth from Smeared Images*", by *Rajiv Kumar Bajpai*, has been carried out under our supervision and that this work has not been submitted elsewhere for the award of a degree.

(Dr. K. S. Venkatesh)
Deptt of Electrical Engineering,
Indian Institute of Technology,
Kanpur.

(Dr. Sumana Gupta)
Deptt of Electrical Engineering,
Indian Institute of Technology,
Kanpur.

To My Parents,
Who gave me a desire for knowledge

Acknowledgments

I would like to thank to my thesis supervisors for their best guidance, advice, tolerance and continuous encouragement during the thesis work and more than anything else their faith in me. I will cherish my association with them for years to come. They have allowed me to learn and pursue various other interests of mine without any interference and i am very happy to have been their student.

I am indebted to my parents whose inspiration and upbringing could bring me to the portals of my present achievement. I am thankful to my friends especially Kaushal, Amitava, Ashwani, and Vinay whose encouragement and continuous interaction lead me to successful completion of my thesis. Special thanks goes to Ramana, Rajrup and Prithwijit who helped me in using frame grabber board.

Finally I am thankful to Bhagvan, without His blessing nothing would have been possible.

Rajiv Kumar Bajpai

Abstract

A method for estimating velocity from two successive frames of motion smeared images is described. The problem is posed as a system identification problem. The underlying phenomenon of motion smearing is modeled as a linear system with an appropriate transfer function. An algorithm for estimating the transfer function is derived. The motion vector is estimated from the support of the corresponding point spread function. Further, a new method for estimating depth and motion simultaneously is presented. The method uses the defocus and the motion-smear information present in the image frames. Both the methods are tested on simulated images.

Contents

List of Figures

Chapter 1

Introduction

It is well known that the visual system sums signals over time, (about 120 ms) in daylight. Although this summation has the advantage of enhancing visual sensitivity, it creates the potential problem of motion blur when viewing moving targets[1]. If the object is moving at a very high speed then, due to integration, motion blur is inevitable. It has also been reported that when the Human Visual System (HVS) is presented with an image, blurred due to motion, the amount of smear perceived by human observers increases with observing durations (up to 20-30ms), but at longer durations, the perceived smear actually decreases, i.e, the perceived image becomes sharper[1]. It appears that the HVS is performing a deblurring operation on the image. For deblurring, a knowledge of motion parameters is required. Hence, it can be concluded that motion smear information is probably used for motion sensation and motion deblurring in the HVS.

In the context of image analysis, however, motion smear has always been considered as a degradation. A large amount of works have been done to remove this degradation [8]. But its positive aspect has always been neglected. Very little work has been done to exploit the positive side of this phenomenon, i.e, to use motion smear as a visual cue for image motion estimation.The first attempt of its kind has been reported in [2] where motion is estimated using motion blur.

We establish a computational model that functionally emulates the behavior of the HVS, i.e, estimates image motion from motion smear information or, in short, "motion-from-smear." We further tried to investigate the possibility of estimating motion and depth simultaneously. For this we studied the defocus blur and motion blur simultaneously. The work described in this thesis is an attempt to explore the positive side of two degradations (a) motion blur and (b) defocus blur, which one always tries to remove. In this work we extract two very important parameters from these degradation, i.e, motion

and depth.

1.1 Motion Smear

It is assumed that image is acquired by keeping the shutter open for an infinitesimally short duration of time, i.e, the shutter speed is very fast. This assumption holds good in many cases where image plane velocities are small relative to the image integration duration, but it fails in situations when available illumination levels are low. In such situations the shutter must be kept open long enough to ensure the integration of sufficient number of photons per pixel to produce images of adequate SNR. If the object moves with very high velocity, then it may cover appreciable distance during exposure time resulting in blurred image of the object. This motion blur is generally referred as *motion smear* in literature.

1.1.1 Image Motion Estimation

Previous research in motion estimation is based on two approaches : Gradient based and Region matching. Different variants exist for each approach, e.g, spatio-temporal approach for gradient-based techniques and recursive region matching for feature-based techniques.

Most gradient-based techniques depend on the relationship between the spatial derivatives and temporal derivatives in time-varying imagery. In order to apply gradient-based techniques to practical situations the image motions must be small and apparent texture must be fine grained. But smaller motions are difficult to detect reliably in the presence of image noise.

In region matching methods, a small sub-region in an image frame is considered. Within the sub-region, a search for the displacement which produces the best match among possible regions in the subsequent frame is evaluated. Feature-based techniques have the advantage of depending on complex image structures that can be detected in conjunction with noise suppression operations. Further, they can be applied to long-range motion situations, i.e., when the image plane velocities are large.

1.1.2 Motion Estimation from Motion Smear

Estimating motion from motion smear is fundamentally different from the families of existing motion estimation methods. It uses an alternative visual cue - motion

smear, while all other methods rely, directly or indirectly, on the conventional cue-displacement. This fundamental difference causes "motion-from-smear" to behave differently from the families of existing techniques. "Motion-from-smear" provides techniques applicable to motion of longer range than gradient-based techniques and, at the same time, applicable to imagery obtained using practical shutter speeds.

In the thesis we first introduce a data acquisition scheme and a model for motion smear. Based on this, we develop a method to get motion parameters by utilizing the *parametric system identification* framework. We formulate the problem as that of finding an appropriate blurring operator, which transforms the local region image with *less smear* into the local region image with *more smear* information. The problem now can be expressed in terms of identification of a pertinent linear system. We further try to incorporate defocus blur in the model to estimate motion and depth simultaneously. For this a new scheme for data acquisition is introduced and by using parametric system identification approach we tried to get both the motion and depth parameters simultaneously.

1.2 Organisation of the Thesis

The work carried out in this thesis is organized as follows. The work has been divided into two parts. The first part is concerned with motion estimation from motion-smeared images, while in the second part of the thesis, an attempt has been made to estimate motion parameters and depth simultaneously from motion smeared images which are also defocused by different amounts.

The second chapter deals with the mathematical formulation of the problem of motion estimation from two successive smeared images. The problem of motion estimation is posed as system identification and appropriate parametric transfer functions are derived. Finally analytical expressions are derived for computing displacements from the polynomial transfer function coefficients.

Chapter three is concerned about system identification algorithms. We discuss the motion-smear model under noisy condition. We also discuss the effect of filter order and window size on the performance of the algorithm developed.

In chapter four, we consider the restoration of blurred image from motion information obtained in the previous chapter. We study the problem of inverse filtering as applied to image restoration. The use of regularized filter for restoration is also discussed.

Chapter five is devoted to simultaneous recovery of motion and depth. Firstly, we introduce a new data acquisition strategy to tackle the problem followed by solving the problem under the framework of system identification described in chapter three for motion estimation.

In chapter six, we discuss the simulation and experimental results obtained by applying the algorithms developed in the previous chapters to simulated test images.

Chapter 2

Mathematical Formulation of the Problem of Motion Estimation from Motion-Smear

2.1 Image Sequence Acquisition

We adopt the same method for acquiring image sequences as explained in [2]. It is as follows:

Let $f(x, y; t)$ denote an ideal, unblurred image at time t. Further, suppose we have an imaging system with a non instantaneous shutter mechanism, i.e., a nonzero exposure time Δt, and denote the observed image by $g(x, y; t, \Delta t)$. Thus, $g(x, y; t_i, \Delta t_{i,i+1})$ is obtained by the shutter opening at time t_i and the sensor integrating the signal until time $t_{i+1} = t_i + \Delta t_{i,i+1}$ for each (x, y). The subscripts of Δt denote the times when the shutter opens and the time when the shutter closes. We assume that the next observation begins immediately, so that at time $t_{i+2} = t_{i+1} + \Delta t_{i+1,i+2}$, $g(x, y; t_{i+1}, \Delta t_{i+1,i+2})$ is available for analysis. Fig. 2.1 illustrates the situation.

2.2 Linear System Model for Motion Smear

Motion smear is modeled as

$$g(x, y; t_i, \Delta t_{i,i+1}) = \frac{1}{\Delta t_{i,i+1}} \int_{t_i}^{t_{i+1}} f(x, y; t) l(t; t_i, \Delta t_{i,i+1}) dt \tag{2.1}$$

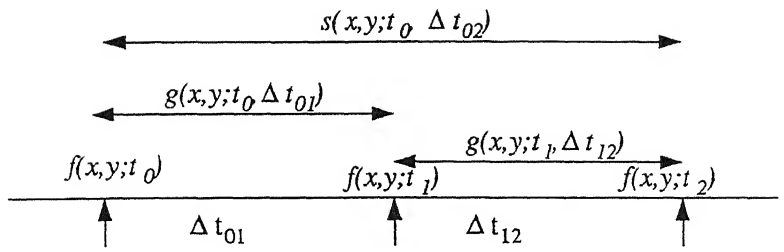

Figure 2.1: Graphical description of data acquisition. The original unblurred image at time t_i is denoted by $f(x, y; t_i)$. The shutter remains open for time interval $\Delta t_{i,i+1}$. The blurred image is denoted by $g(x, y; t_i, \Delta t_{i,i+1})$. $s(x, y; t_i, \Delta t_{i,i+2})$ would be the image acquired if ther camera shutter were kept open from t_i to t_{i+2}.

where $l(t; t_i, \Delta t_{i,i+1})$ is the transmission coefficient of the lens/filter system. If the image motion is translational then

$$f(x, y; t) = \int_{-\infty}^{\infty} \int_{-\infty}^{\infty} f(\alpha, \beta; t_i)\delta(x - v_x(t - t_i) - \alpha, y - v_y(t - t_i) - \beta)d\alpha d\beta \quad (2.2)$$

where $t \in (t_i, t_{i+1}]$ and $\mathbf{v} = (v_x, v_y)$ is the image motion vector at (x, y). From equations (2.1) and (2.2) we get

$g(x, y; t_i, \Delta t_{i,i+1}) =$

$\frac{1}{\Delta t_{i,i+1}} \int_{t_i}^{t_{i+1}} (\int_{-\infty}^{\infty} \int_{-\infty}^{\infty} f(\alpha, \beta; t_i)\delta(x - v_x(t - t_i) - \alpha, y - v_y(t - t_i) - \beta)d\alpha d\beta)$
$l(t, t_i, \Delta t_{i,i+1})dt$

$=$

$\frac{1}{\Delta t_{i,i+1}} \int_{-\infty}^{\infty} \int_{-\infty}^{\infty} f(\alpha, \beta; t_i)(\int_{t_i}^{t_{i+1}} \delta(x - v_x(t - t_i) - \alpha, y - v_y(t - t_i) - \beta)l(t; t_i, \Delta t_{i,i+1})dt)$
$d\alpha d\beta$

If

$$h(x, y, \alpha, \beta; t_i, \Delta t_{i,i+1}; \mathbf{v}) =$$

$$\frac{1}{\Delta t_{i,i+1}} \int_{t_i}^{t_{i+1}} \delta(x - v_x(t - t_i) - \alpha, y - v_y(t - t_i) - \beta)l(t; t_i, \Delta t_{i,i+1})dt \quad (2.3)$$

then

$$g(x, y; t_i, \Delta t_{i,i+1}) = \int_{-\infty}^{\infty} \int_{-\infty}^{\infty} f(\alpha, \beta; t_i)h(x, y, \alpha, \beta; t_i, \Delta t_{i,i+1}; \mathbf{v})d\alpha d\beta \quad (2.4)$$

This is a generalization of the linear system model for motion smear that is generally used in image restoration. Here $h(.)$ is a blurring operator known as point spread

function (PSF). We take the sensor gain $l(.)$ as unity over the shutter opening duration, which is the well known boxcar model used in image restoration [8]. Then the PSF equation (2.3) reduces to

$$h(x, y, \alpha, \beta; t_i, \Delta t_{i,i+1}; \mathbf{v}) = \int_{t_i}^{t_{i+1}} \delta(x - v_x(t - t_i) - \alpha, y - v_y(t - t_i) - \beta)dt \quad (2.5)$$

The motion vector is known if $h(.)$ is available because the support of the $h(.)$ is uniquely determined by $\mathbf{v}$. In general, $h(.)$ is space-varying in nature but it may be assumed as locally space-invariant. It is also assumed in the above model that $\mathbf{v}$ doesn't change during $(t_i, t_{i+1}]$(uniform motion).

Consider two successive motion smeared frames at $i = 0, 1$. We further assume that $\mathbf{v}$ is constant over time intervals of the order of $\Delta t_{01} + \Delta t_{12}$.
If we take the space-invariant linear system model, we get

$$\begin{aligned} g(x, y; t_0, \Delta t_{01}) &= f(x, y; t_0) \star h(x, y; t_0, \Delta t_{01}; \mathbf{v}) \\ &= f(x, y; t_0) \star h_{01}(x, y; \mathbf{v}) \end{aligned} \quad (2.6)$$

and

$$\begin{aligned} g(x, y; t_1, \Delta t_{12}) &= f(x, y; t_1) \star h(x, y; t_1, \Delta t_{12}; \mathbf{v}) \\ &= f(x, y; t_1) \star h_{12}(x, y; \mathbf{v}) \end{aligned} \quad (2.7)$$

In the space-invariant case, equation (2.2) simplifies to

$$\begin{aligned} f(x, y; t_1) &= f(x, y; t_0) \star \delta(x - v_x \Delta t_{01}, y - v_y \Delta t_{01}) \\ &= f(x, y; t_0) \star \delta(x - L_x, y - L_y) \end{aligned}$$

where

$$\begin{aligned} L_x &= v_x \Delta t_{01} \\ L_y &= v_y \Delta t_{01} \end{aligned}$$

Now we create the sum signal defined as

$$s(x, y; t_0, \Delta t_{02}) = g(x, y; t_0, \Delta t_{01}) + g(x, y; t_1, \Delta t_{12}) \quad (2.8)$$

or briefly,

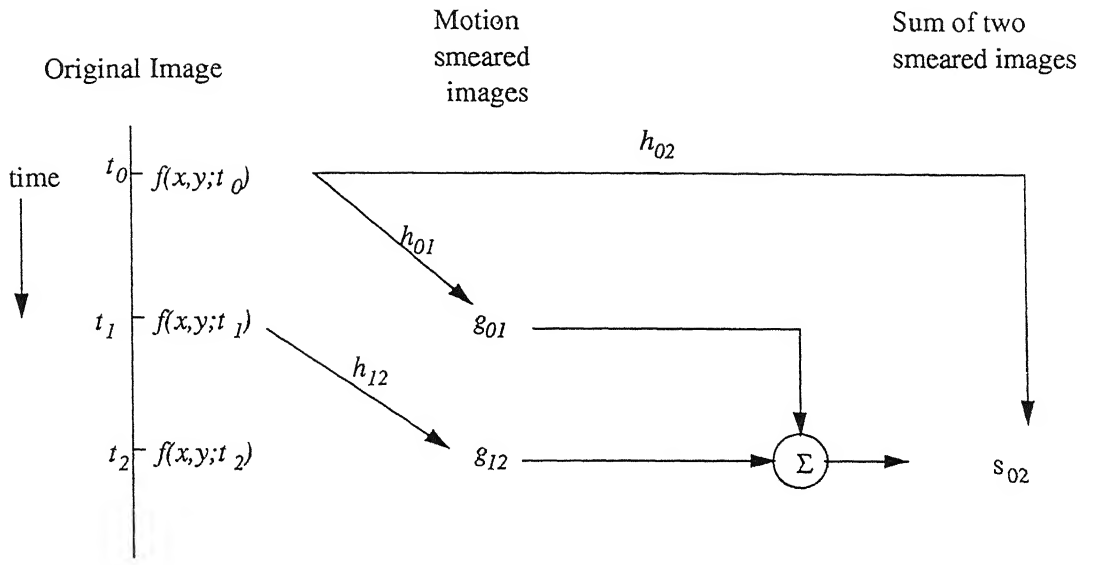

Figure 2.2: The meaning of $s_{02}(x, y; t_0, \Delta t_{02})$ and $h_{02}(x, y; \mathbf{v})$

$$\begin{aligned} s_{02} &= g_{01} + g_{12} \\ &= f_0 \star h_{01} + f_1 \star h_{12} \\ &= f_0 \star h_{01} + f_0 \star h' \star h_{12}; \text{where } h' = \delta(x - L_x, y - L_y); \\ &= f_0 \star (h_{01} + h' \star h_{12}) \\ s_{02} &= f_0 \star h_{02} \\ \text{where, } h_{02} &= h_{01} + h' \star h_{12} \end{aligned} \tag{2.9}$$

Here we have used the shorthand notation g_{01}, g_{12} s_{02}, h_{01}, h_{12} for $g(x, y; t_0, \Delta t_{01})$, $g(x, y; t_1, \Delta t_{12})$, $s(x, y; t_0, \Delta t_{02})$, $h_{01}(x, y; \mathbf{v})$, $h_{12}(x, y; \mathbf{v})$ respectively. we note that s_{02} corresponds to the blurred image acquired if the camera shutter were kept open from t_0 to t_2 (Note: Here we left averaging factor $\frac{1}{2}$ in equation (2.9) for simplicity). Since the PSFs are space varying, thus all the above results are only locally valid. The Fig. 2.2 illustrates the above equation.

2.3 Motion Estimation as System Identification

In frequency domain we can write from equations (2.6), (2.7) and (2.9)

$$G_{01}(\Omega_x, \Omega_y; t_0, \Delta t_{01}) = F_0(\Omega_x, \Omega_y) H_{01}(\Omega_x, \Omega_y; \mathbf{v}) \tag{2.10}$$

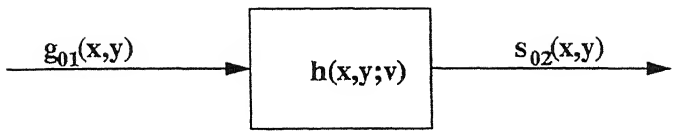

Figure 2.3: The block diagram of the underlying system

$$\begin{aligned} S_{02}(\Omega_x, \Omega_y; t_0, \Delta t_{02}) &= F_0(\Omega_x, \Omega_y) H_{02}(\Omega_x, \Omega_y; \mathbf{v}) \\ &= F_0(\Omega_x, \Omega_y)(H_{01}(\Omega_x, \Omega_y) + H'(\Omega_x \Omega_y) H_{12}(\Omega_x, \Omega_y)) \end{aligned} \tag{2.11}$$

Let the two exposure duration $\Delta t_{01}$and Δt_{12} be the same, we have

$$\begin{aligned} H_{01}(\Omega_x, \Omega_y) = H_{12}(\Omega_x, \Omega_y) &= \frac{sin(\frac{\Omega L}{2})}{\frac{\Omega L}{2}} e^{-j\frac{\Omega L}{2}} \\ \text{where,} \quad \Omega L &= \Omega_x L_x + \Omega_y L_y \end{aligned} \tag{2.12}$$

Further,

$$H'(\Omega_x, \Omega_y) = \mathrm{FT}\{h'(x, y; \mathbf{v})\} = exp(-j\Omega L) \tag{2.13}$$

Hence from equations (2.11), (2.12) and (2.13) we have

$$\begin{aligned} S_{02}(\Omega_x, \Omega_y) &= F_0(\Omega_x, \Omega_y) H_{01}(\Omega_x, \Omega_y)(1 + exp(-j\Omega L)) \\ &= G_{01}(\Omega_x, \Omega_y)(1 + \exp(-j\Omega L)) \end{aligned} \tag{2.14}$$

If

$$H(\Omega_x, \Omega_y) = 1 + \exp(-j\Omega L) \tag{2.15}$$

then from equation (2.14) we have

$$S_{02}(\Omega_x, \Omega_y) = H(\Omega_x, \Omega_y) G_{01}(\Omega_x, \Omega_y) \tag{2.16}$$

$$H(\Omega_x, \Omega_y) = \frac{S_{02}(\Omega_x, \Omega_y)}{G_{01}(\Omega_x, \Omega_y)}$$

$$\text{or,} \quad s_{02}(x, y) = h(x, y; v) \star g_{01}(x, y) \tag{2.17}$$

where

$$h(x, y; \mathbf{v}) = \delta(x, y) + \delta(x - L_x, y - L_y) \tag{2.18}$$

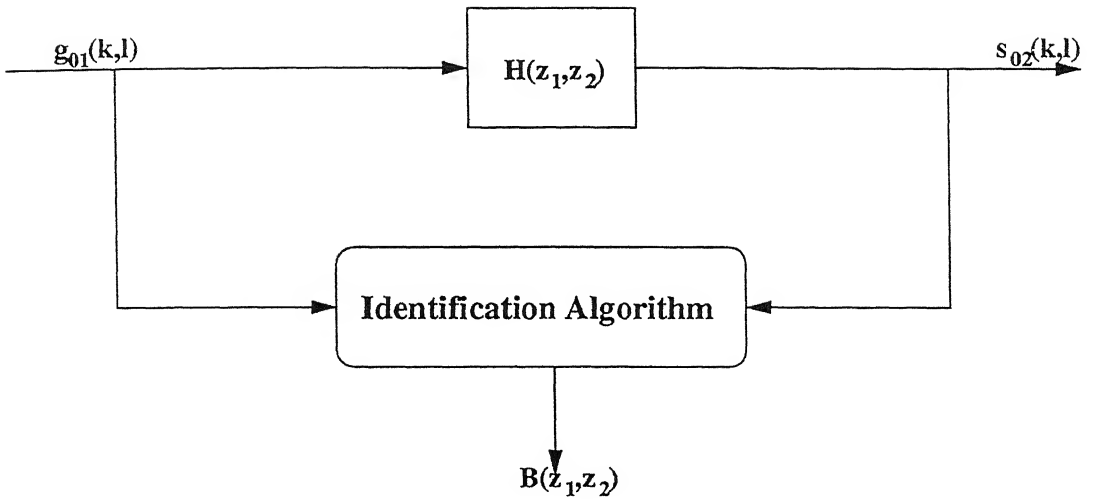

Figure 2.4: System identification

Fig. 2.3 shows the block diagram where $g_{01}(x, y)$ is the input of a linear system whose output is $s_{02}(x, y)$ (Note: the time dependence of the notations for $g_{01}(.)$ and $s_{02}(.)$ have been dropped for convenience).

Equation (2.17) represents a linear system with $h(x, y; \mathbf{v})$ as the impulse response. Assuming local space invariance, the motion estimation problem can be framed as a system identification problem, where given the observations of the input $\{g_{01}\}$ and output $\{s_{02}\}$, we have to identify certain parameters of the underlying system. The derivation of the relevant system description from the observed images needs a model to describe the system and an identification procedure to estimate the parameters of the model. This in turn will provide the relevant information we wish to infer about the system.

2.4 Parameterization of the Transfer Function

In order to estimate motion, we need to approximate $H(\Omega_x, \Omega_y)$ by some parametric function i.e find a function $B(\Omega_x, \Omega_y)$ which approximates $H(\Omega_x, \Omega_y)$ by minimizing an appropriate cost function through an identification algorithm as shown in Fig. 2.4.

Equation (2.16) models the underlying process in the continuous domain. However, in practice, only digitized images are available, therefore we have to find an appropriate parameterization of the transfer function which will enable us to obtain the parameters from those digitized images. Let $g_{01}(k, l)$, $s_{02}(k, l)$ and $h(k, l)$ be the sampled signals corresponding to $g_{01}(x, y)$,$s_{02}(x, y)$ and $h(x, y; \mathbf{v})$ respectively. The sampled signals are related in Fourier domain as

$$H(\omega_1, \omega_2) = \frac{S_{02}(\omega_1, \omega_2)}{G_{01}(\omega_1, \omega_2)} \tag{2.19}$$

where $S_{02}(\omega_1, \omega_2)$, $G_{01}(\omega_1, \omega_2)$ and $H(\omega_1, \omega_2)$ are the Fourier transforms of the sequences $s_{02}(k, l)$, $g_{01}(k, l)$ and $h(k, l)$ respectively. Now we reformulate the problem as that of approximating the transfer function $H(\omega_1, \omega_2)$ of the underlying system with an appropriate parametric transfer function $B(\omega_1, \omega_2)$.

Since equation (2.15) suggests that the unknown transfer function $H(\omega_1, \omega_2)$ is of polynomial form, it is approximated with non-causal polynomial transfer function with b_{mn} as coefficients, i.e.

$$B(\omega_1, \omega_2) = \sum_{m=-M}^{M} \sum_{n=-M}^{M} b_{mn} e^{-j\omega_1 m} e^{-j\omega_2 n} \tag{2.20}$$

2.5 Analytical Expression for the Displacements

We have,

$$H(\omega_1, \omega_2) = FT\{h(k, l)\} = FT\{h(m\Delta T, n\Delta T)\} = 1 + \exp(-j\omega L) \tag{2.21}$$
$$\text{where,} \quad \omega L = \omega_1 L_x + \omega_2 L_y$$

Now taking the partial derivative of equation (2.21) and evaluating it at $\omega_1 = \omega_2 = 0$, we get

$$\begin{aligned} \left.\frac{\partial H(\omega_1, \omega_2)}{\partial \omega_1}\right|_{\omega_1=\omega_2=0} &= (-jL_x)(\exp(-j\omega_1 L_x)\exp(-j\omega_2 L_y))|_{\omega_1=\omega_2=0} \\ &= (-jL_x) \\ \left.\frac{\partial H(\omega_1, \omega_2)}{\partial \omega_2}\right|_{\omega_1=\omega_2=0} &= (-jL_y)(\exp(-j\omega_1 L_x)\exp(-j\omega_2 L_y))|_{\omega_1=\omega_2=0} \\ &= (-jL_y) \end{aligned} \tag{2.22}$$

If we take the partial derivative of $B(\omega_1, \omega_2)$, we get

$$\left.\frac{\partial B(\omega_1, \omega_2)}{\partial \omega_1}\right|_{\omega_1=\omega_2=0} = -j\left(\sum_{m=-M}^{M} \sum_{n=-M}^{M} m b_{mn}\right)$$

$$\left.\frac{\partial B(\omega_1,\omega_2)}{\partial \omega_2}\right|_{\omega_1=\omega_2=0} = -\jmath\Big(\sum_{m=-M}^{M}\sum_{m=-M}^{M} nb_{mn}\Big) \tag{2.23}$$

Hence from equation (2.22) and (2.23) we get analytical expression of displacements during shutter opening time as

$$\begin{aligned} L_x &= \Big(\sum_{m=-M}^{M}\sum_{n=-M}^{M} mb_{mn}\Big) \\ L_y &= \Big(\sum_{m=-M}^{M}\sum_{n=-M}^{M} nb_{mn}\Big) \end{aligned} \tag{2.24}$$

One way of interpreting equation (2.24) is that displacements are the first moment of transfer function(i.e $h(x, y; \mathbf{v})$) about x and y axis respectively in our case. Hence once the coefficients of the transfer functions are approximated by some suitable algorithm, we can easily estimate displacements analytically.

Chapter 3

Identification of Transfer Function Coefficient

System Identification or the process of constructing an approximation to the underlying transfer function of a system from the input-output measurements has a rich history and is a well studied problem. It is one of the central tools used in signal processing and control theory. Construction of an approximation to the underlying transfer function of a system requires four things, viz,

- The Input-Output measurement record.
- An appropriate Model for the transfer function.
- A cost function which characterizes how close the model is to the transfer function.
- An algorithm to identify the parameters by minimizing the cost function.

The extraction of any relevant description about the system is limited by the input-output measurements. These measurements may be contaminated by noise or there may not be enough information present in them for proper identification. These factors affect the accuracy of the identified parameters.

As discussed in the previous chapter, the appropriate model for the transfer function to be approximated is a non-causal polynomial in our case. Though it can also be approximated by rational transfer function, but in our work we used only polynomial transfer function approximation.

The cost function quantifies the closeness between the model and the underlying transfer function. Assuming that a model is available, a best approximation is obtained by minimizing the cost function in the parameters. In general, the cost function is chosen such that it is convex and has a unique global minimum. One such function is the quadratic error criterion in which the sum of the squared errors is minimized, which is known as the least mean squares error criterion.

The parameters are obtained by minimizing the cost function through an appropriate algorithm. The choice of algorithm is determined by its ability to converge to the global minimum and by its computational complexity. In the following we develop equation error algorithms for the minimization of the quadratic cost function to identify the coefficients of the polynomial transfer functions.

3.1 Equation Error Method

Consider the parametric transfer function defined by the equation (2.20). Substituting it in (2.16) and rearranging the terms we get

$$\widehat{S}_{02}(\omega_1,\omega_2) = \sum_{m=-M}^{M}\sum_{n=-M}^{M} b_{mn} G_{01}(\omega_1,\omega_2)\exp(-j\omega_1 m)\exp(-j\omega_2 n) \tag{3.1}$$

where $\widehat{S}_{02}(\omega_1,\omega_2)$ is the reconstruction of $S_{02}(\omega_1,\omega_2)$. Taking the inverse Fourier Transform, we have

$$\begin{aligned} \widehat{s}_{02}(k,l) &= \sum_{m=-M}^{M}\sum_{n=-M}^{M} b_{mn} g_{01}(k-m,l-n) \\ &\quad \text{for all k, l} \end{aligned} \tag{3.2}$$

where the output is modeled as moving-averages of the input. We now define equation error signal [3] as

$$\begin{aligned} e(k,l) &= s_{02}(k,l) - \widehat{s}_{02}(k,l) \\ e(k,l) &= s_{02}(k,l) - \sum_{m=-M}^{M}\sum_{n=-M}^{M} b_{mn} g_{01}(k-m,l-n); \\ &\quad \text{for all k, l} \end{aligned} \tag{3.3}$$

The flow of the equation error signal is shown in Fig.3.1. The equation error can be

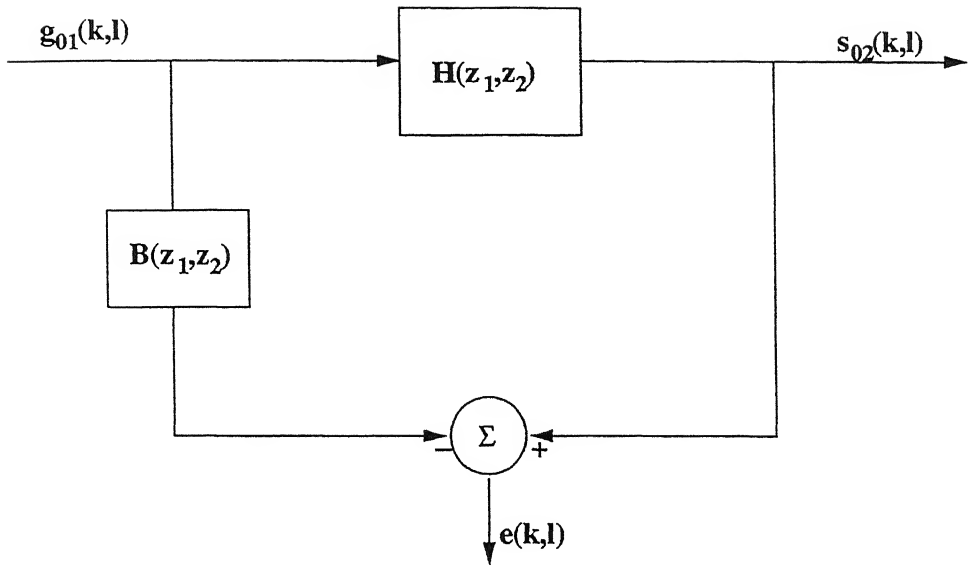

Figure 3.1: The flow diagram of equation error signal

written in terms of lexicographically ordered vectors as

$$e(k,l) = \begin{bmatrix} -\mathbf{b}^T & 1 \end{bmatrix} \begin{bmatrix} \mathbf{g_{01}}(k,l) \\ s_{02}(k,l) \end{bmatrix} \tag{3.4}$$

or if $\mathbf{a}^t = [0\,0 \ldots\ldots 1 \ldots\ldots 0\,0]$ then equation (3.4) can be rewritten as

$$e(k,l) = \begin{bmatrix} -\mathbf{b}^T & \mathbf{a}^T \end{bmatrix} \begin{bmatrix} \mathbf{g_{01}}(k,l) \\ \mathbf{s_{02}}(k,l) \end{bmatrix} \tag{3.5}$$

where $\mathbf{b}$ is a vector of length K, obtained by stacking the columns of the coefficient matrix into a vector form given by

$$\mathbf{b}^T = [b_{-M,-M} \ldots\ b_{M,-M} \ldots b_{0,0} \ldots\ldots b_{-M,M} \ldots b_{M,M}]$$

and the vectors $\mathbf{g_{01}}$, $\mathbf{s_{02}}$ is obtained by stacking the columns of $L \times L$ matrix extracted from the input local region image around the point (k,l) with $L = 2M+1$ and $K = L^2$.

$$\begin{aligned} \mathbf{g_{01}}^T(k,l) \;=\; & [g_{01}(k+M,l+M) \ldots\ldots g_{01}(k-M,l+M) \ldots\ldots \\ & \ldots\ldots g_{01}(k,l) \ldots g_{01}(k+M,l-M) \ldots \\ & \ldots\ldots g_{01}(k-M,l-M)] \end{aligned}$$

$$\mathbf{s_{02}}^T(k,l) \;=\; [s_{02}(k+M,l+M) \ldots\ldots s_{02}(k-M,l+M) \ldots\ldots$$

$$.....s_{02}(k,l)\,...s_{02}(k+M,l-M)\,...$$
$$....s_{02}(k-M,l-M)]$$

The variance of the equation error given by equation (3.5) is easily found as

$$E[e^2(k,l)] = \begin{bmatrix} -\mathbf{b}^T & \mathbf{a}^T \end{bmatrix} \begin{bmatrix} \mathbf{R}_{gg}(k,l) & \mathbf{R}_{gs}(k,l) \\ \mathbf{R}_{gs}^T(k,l) & \mathbf{R}_{ss}(k,l) \end{bmatrix} \begin{bmatrix} -\mathbf{b} \\ \mathbf{a} \end{bmatrix} \tag{3.6}$$

where

$$\begin{aligned} \mathbf{R}_{gg}(k,l) &= E[\mathbf{g_{01}}(k,l)\mathbf{g_{01}}^T(k,l)] \\ \mathbf{R}_{gs}(k,l) &= E[\mathbf{g_{01}}(k,l)\mathbf{s_{02}}^T(k,l)] \\ \mathbf{R}_{ss}(k,l) &= E[\mathbf{s_{02}}(k,l)\mathbf{s_{02}}^T(k,l)] \end{aligned} \tag{3.7}$$

where $E(.)$ is the expectation operator and $\mathbf{R}_{gg}$, $\mathbf{R}_{gs}$ and $\mathbf{R}_{ss}$ are the signal correlation matrices. Further, assuming the signals of interest to be stationary, the spatial dependence of correlation matrices will be suppressed.

We assume that the input image over a local region around a given point is stationary, ergodic and persistently exciting of sufficient degree[3], such that $\mathbf{R}_{gg}$ is invertible.We can then use a matrix identity

$$\begin{aligned} \begin{bmatrix} \mathbf{R}_{gg} & \mathbf{R}_{gs} \\ \mathbf{R}_{gs}^T & \mathbf{R}_{ss} \end{bmatrix} &= \begin{bmatrix} \mathbf{I} & \mathbf{0} \\ \mathbf{R}_{gs}^T\mathbf{R}_{gg}^{-1} & \mathbf{I} \end{bmatrix} \begin{bmatrix} \mathbf{R}_{gg} & \mathbf{0} \\ \mathbf{0} & \mathbf{R}_{ss} - \mathbf{R}_{gs}^T\mathbf{R}_{gg}^{-1}\mathbf{R}_{gs} \end{bmatrix} \\ &\quad \times \begin{bmatrix} \mathbf{I} & \mathbf{R}_{gg}^{-1}\mathbf{R}_{gs} \\ \mathbf{0} & \mathbf{I} \end{bmatrix} \end{aligned} \tag{3.8}$$

which gives a block triangular LDU factorization. All the matrices in the above equation are of dimension $K \times K$. At first sight, this factorization looks formidable, but of particular interest is a term in the center factor:

$$\mathbf{R}_{s/g} = \mathbf{R}_{ss} - \mathbf{R}_{gs}^T\mathbf{R}_{gg}^{-1}\mathbf{R}_{gs} \tag{3.9}$$

This is called the Schur complement of $\mathbf{R}$ with respect to $\mathbf{R}_{gg}$. Note that $\mathbf{R}$ is

$$\mathbf{R} = \begin{bmatrix} \mathbf{R}_{gg} & \mathbf{R}_{gs} \\ \mathbf{R}_{gs}^T & \mathbf{R}_{ss} \end{bmatrix}$$

From equations (3.8) and (3.9) we have,

$$E[e^2(k,l)] = \mathbf{a}^T\mathbf{R}_{s/g}\mathbf{a} + [-\mathbf{b} + \mathbf{R}_{gg}^{-1}\mathbf{R}_{gs}\mathbf{a}]^T\mathbf{R}_{gg}[-\mathbf{b} + \mathbf{R}_{gg}^{-1}\mathbf{R}_{gs}\mathbf{a}] \tag{3.10}$$

Now minimizing equation (3.10) with respect to the vector $\mathbf{b}$ gives

$$\begin{aligned} \mathbf{b} &= \mathbf{R}_{gg}^{-1}\mathbf{R}_{gs}\mathbf{a} \\ \text{or, } \mathbf{b} &= \mathbf{R}_{gg}^{-1}\mathbf{r}_{gs} \text{ where } \mathbf{r}_{gs} = \mathbf{R}_{gs}\mathbf{a} \end{aligned} \tag{3.11}$$

Once we obtain vector $\mathbf{b}$ as discussed above we can get velocity vector $\mathbf{v}$ using equation (2.24).

3.2 Dealing with Noise

The model described in the previous chapter is the noise free case i.e, we have assumed the observed images are noise free. Since such an assumption is impractical in real situation, we consider the model for motion-smear under noisy image frames and show how well suited the equation error identification algorithm is to approximate the polynomial transfer function under noisy condition.
Let us consider the noise corrupted versions of $g(x, y; t_i, \Delta t_{i,i+1})$ as,

$$g_n(x, y; t_0, \Delta t_{01}) = g(x, y; t_0, \Delta t_{01}) + n(x, y; t_0) \tag{3.12}$$

and

$$g_n(x, y; t_1, \Delta t_{12}) = g(x, y; t_1, \Delta t_{12}) + n(x, y; t_1) \tag{3.13}$$

where $n(x, y; t_0, \Delta t_{01})$ and $n(x, y; t_1, \Delta t_{12})$ are zero-mean, white Gaussian noise.

The noisy sum signal $s_n(x, y; t_0, \Delta t_{02})$ is defined as

$$\begin{aligned} s_{02_n}(x, y) &= g_{01_n}(x, y) + g_{12_n}(x, y) \\ &= g_{01}(x, y) + g_{12}(x, y) + n_0(x, y) + n_1(x, y) \\ &= s_{02}(x, y) + n_2(x, y) \end{aligned} \tag{3.14}$$

Here we have used notations $s_{02_n}(.)$, $g_{01_n}(.)$, $g_{12_n}(.)$,$n_0(.)$ and $n_1(.)$ to denote for noisy version of the signals and noise. We leave the time dependence of notation for convenience. Note that $n_2(x, y)$ is a zero-mean Gaussian noise.

From equation (2.17), we see that under noise free condition $s_{02}(x, y)$ is given as

$$s_{02}(x, y) = h(x, y; v) \star g_{01}(x, y) \tag{3.15}$$

Hence, we can model the system in the noisy case as

$$s_{02_n}(x, y) = h(x, y; v) \star g_{01}(x, y) + n_2(x, y) \tag{3.16}$$

The acquired noisy $g_{01_n}(x, y)$ needs to be denoised by some prefiltering operation to get $\widehat{g}_{01}(x, y) \cong g_{01}(x, y)$. Two feasible solution are considered for the noisy case:

1. Denoise both the input $g_{01}(x, y)$ and output $s_{02}(x, y)$ frames and then do the motion estimation.This is the noise free case as discussed in the previous chapter.

2. Denoise the input frame $g_{01_n}(x, y)$ to get $\widehat{g}_{01}(x, y) \cong g_{01}(x, y)$ and then approximate the motion parameters under system identification frame work, using model described by equation (3.16).

The system model described by equation (3.16) is the one which is generally used in system identification by equation error method[3]. The method discussed in the previous section is one of its case when $n_2(x, y) = 0$. In the following sub-section, we will show that if we adopt the model described by equation (3.16), then the estimated polynomial coefficient $\mathbf{b}$ will remain unaffected by the output noise $n_2(x, y)$.

3.2.1 Estimation of polynomial transfer function coefficients

Fig. 3.2 shows the signal flow graph of the equation error identifier. Here $H(z_1, z_2)$ is the unknown polynomial transfer function to be identified, driven by a preprocessed input $\{\widehat{g}_{01}(k, l)\}$ and whose output $\{s_{02}(k, l)\}$ is corrupted by a Gaussian disturbance $\{n_2(k, l)\}$ which is assumed statistically independent of the input.
The equation error whose variance is to be minimized is

$$e(k, l) = \begin{bmatrix} -\mathbf{b}^T & \mathbf{a}^T \end{bmatrix} \begin{bmatrix} \widehat{\mathbf{g}}_{01} \\ \mathbf{s}_{02_n} \end{bmatrix} \tag{3.17}$$

where $\mathbf{b}^T$, $\widehat{\mathbf{g}}_{01}$ and $\mathbf{s}_{02_n}$ are lexicographically ordered vectors as discussed earlier. Note that here, $\mathbf{a}^T = [0\,0 \ldots\ldots 1 \ldots\ldots\ldots 0\,0]$. The variance of the equation error is easily found as

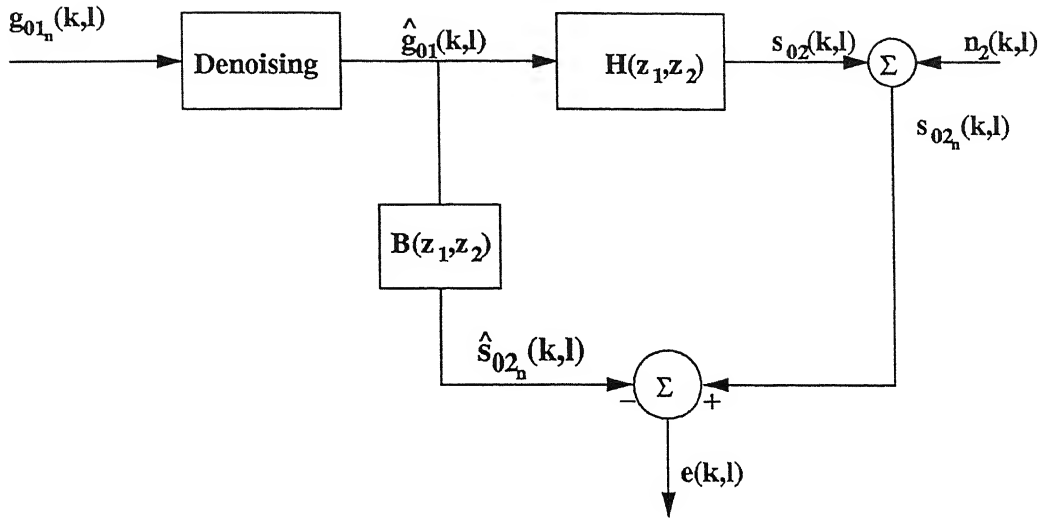

Figure 3.2: Signal flow graph of equation error identifier

$$E[e^2(k,l)] = \begin{bmatrix} -\mathbf{b}^T & \mathbf{a}^T \end{bmatrix} \begin{bmatrix} \mathbf{R}_{\widehat{gg}} & \mathbf{R}_{\widehat{g}s_n} \\ \mathbf{R}_{\widehat{g}s_n}^T & \mathbf{R}_{s_n s_n} \end{bmatrix} \begin{bmatrix} -\mathbf{b} \\ \mathbf{a} \end{bmatrix} \tag{3.18}$$

with

$$\mathbf{R}_{\widehat{gg}} = E\left[\hat{\mathbf{g}}_{01}\hat{\mathbf{g}}_{01}^T\right] = E\left[\mathbf{g}_{01}\mathbf{g}_{01}{}^T\right] = \mathbf{R}_{gg}\,,$$
$$\mathbf{R}_{\widehat{g}s_n} = E\left[\hat{\mathbf{g}}_{01}\mathbf{s}_{02_n}{}^T\right] = E\left[\mathbf{g}_{01}(\mathbf{s}_{02}+\mathbf{n}_2)^T\right] = \mathbf{R}_{gs},$$
$$\mathbf{R}_{s_n s_n} = E\left[\mathbf{s}_{02_n}\mathbf{s}_{02_n}{}^{\mathbf{T}}\right] = \mathbf{R}_{ss} + \sigma_{n_2}^2\mathbf{I},$$

Note that the spatial dependence of the correlation matrices have been suppressed as earlier we did with stationary assumption of the signals.

Now equation (3.18) is further simplified as

$$E[e^2(k,l)] = \begin{bmatrix} -\mathbf{b}^T & \mathbf{a}^T \end{bmatrix} \begin{bmatrix} \mathbf{R}_{gg} & \mathbf{R}_{gs} \\ \mathbf{R}_{gs}^T & \mathbf{R}_{ss} \end{bmatrix} \begin{bmatrix} -\mathbf{b} \\ \mathbf{a} \end{bmatrix} + \sigma_{n_2}^2 \mathbf{a}^T\mathbf{a} \tag{3.19}$$

Since $\mathbf{a}^T\mathbf{a} = 1$, hence equation (3.19) may be rewritten as

$$E[e^2(k,l)] = \begin{bmatrix} -\mathbf{b}^T & \mathbf{a}^T \end{bmatrix} \begin{bmatrix} \mathbf{R}_{gg} & \mathbf{R}_{gs} \\ \mathbf{R}_{gs}^T & \mathbf{R}_{ss} \end{bmatrix} \begin{bmatrix} -\mathbf{b} \\ \mathbf{a} \end{bmatrix} + \sigma_{n_2}^2 \tag{3.20}$$

As we see from equation (3.20) that the presence of noise now adds only a constant term to the equation error variance, so the polynomial coefficient vector $\mathbf{b}^T$, obtained by minimizing the error variance, does not vary with the noise power $\sigma_{n_2}^2$. This is the advantage of using equation error identifier for our estimation purpose.

As derived earlier, the polynomial coefficient is obtained by minimizing the equation

(3.18) which gives

$$\mathbf{b} = \mathbf{R}_{\widehat{gg}}^{-1}\mathbf{R}_{\widehat{gs}_n} = \mathbf{R}_{gg}^{-1}\mathbf{R}_{gs} \tag{3.21}$$

Hence the estimation of coefficient is not affected by background noise power $\sigma_{n_2}^2$ when we adopt the model defined by equation (3.16).

3.3 Filter Order and Window Size

The two parameters of particular importance in this procedure are

1. The choice of filter order determined by M and
2. The window size $N \times N$ of the local region.

The choice of M to determine filter order plays a crucial role in finding b_{mn}. The automatic model order determination in 2-D case through eigen analysis of Schur complement [4] is difficult owing to non-causal nature of model. However, if we assume that maximum displacement of the object is known apriori, then we may be able to fix the model order. A correct choice of M is the least value at which MSE reaches its minimum. This is shown in the chapter 6. The assumption of ergodicity requires a large number of samples (pixels). The resulting increase in window size conflicts with the assumption of space invariance over a local region. An optimal choice of window size is therefore crucial.

If we consider 1-D case of system identification and let $H(z)$ to be approximated by $B(z)$ and both are rational functions of degree M_1, then in order to identify the unknown transfer function $H(z)$ i.e, $B(z) = H(z)$ the input signal $\{u(n)\}$ should be persistently exciting of degree $2M_1 + 1$ (=the number of free parameters) or greater[3]. If $\{u(n)\}$ is persistently exciting of degree less than $2M_1 + 1$, then exact identification of the system is not possible . This concept can be extended to 2-D case and we have taken $N = 4M_{max} + 1$, where M_{max} is the value of M corresponding to maximum displacement, so that in the case of maximum displacement, transfer function can be identified.

3.4 The Complete Algorithm

The overall algorithm for estimating motion from motion-smear model is:

1. Select a location (x_i, y_i) in the images and define an $N \times N$ local region image around that location.

2. Obtain the correct value of M as explained in the section (3.3) so that the approximating transfer function is of sufficient order.

3. Estimate polynomial transfer function coefficient vector $\mathbf{b}$, using *equation error identification algorithm.*

4. Using these coefficients we calculate displacement analytically as discussed in chapter 2.

5. Move to the next image location (x_{i+1}, y_{i+1}) and repeat the above to get the motion parameters at that point.

Chapter 4

Image Restoration

4.1 Image Restoration as Inverse filtering

We have seen in the previous chapter that motion smeared image can be modeled as

$$g(k,l) = f_0(k,l) \star b(k,l) \tag{4.1}$$

where the degraded image $g(k,l)$ is the result of convolving the original image $f_0(k,l)$ with the blurring operator $b(k,l)$. The problem of restoring original image can be classified into two categories. One is the deconvolution problem, in which $b(k,l)$ is assumed to known. The second is the blind deconvolution problem, where $b(k,l)$ is not known and must be estimated from available information. Once the blurring operator is estimated or it is known, we can easily reduce the blur by inverse filtering . From (4.1) we obtain,

$$G(\omega_1,\omega_2) = F_0(\omega_1,\omega_2)B(\omega_1,\omega_2)$$

or

$$F_0(\omega_1,\omega_2) = \frac{G(\omega_1,\omega_2)}{B(\omega_1,\omega_2)} \tag{4.2}$$

Fig. 4.1 illustrates the equation (4.2). The inverse filter in Fig. 4.1 tends to be very sensitive to noise . When $B(\omega_1,\omega_2)$ is very small, $\frac{1}{B(\omega_1,\omega_2)}$ is very large, and small noise in the frequency regions where $\frac{1}{B(\omega_1,\omega_2)}$ is very large may be greatly emphasised.

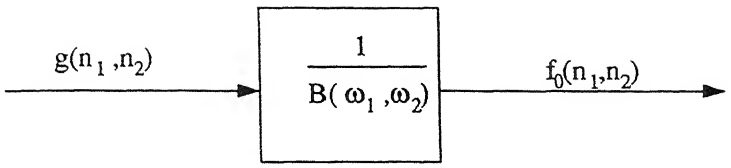

Figure 4.1: Inverse filtering for image restoration.

4.1.1 Regularised inverse filter

An inverse problem is characterised as ill-posed when there is no guarantee for the existence, uniqueness, and stability of the solution based on direct inversion. Several methods have been studied to solve the inverse problem. One such method of lessening the noise sensitivity is to use the regularised inverse filter. We define a regularised inverse filter as

$$H(\omega_1, \omega_2) = \frac{B^*(\omega_1, \omega_2)}{B(\omega_1, \omega_2)B^*(\omega_1, \omega_2) + \gamma} \tag{4.3}$$

where γ is called the *regularizing parameter*. When $\gamma \rightarrow 0$, it becomes the inverse filter as defined in (4.2). Thus, if we choose γ to be very small, we can restore the original image without having any noise amplification problem.

4.2 Image Restoration from Motion Smear Model

Once the blurring operator is estimated, we can restore the original image as discussed in the previous section. As we see from (2.5), the PSF function is given as

$$h(x, y; t_i, \Delta t_{i,i+1}; \mathbf{v}) = \frac{1}{\Delta t_{i,i+1}} \int_{t_i}^{t_{i+1}} \delta(x - v_x(t - t_i), y - v_y(t - t_i))dt \tag{4.4}$$

Its Fourier transform is calculated as

$$H(\Omega_x, \Omega_y; \mathbf{v}) = \frac{2}{\Omega L}.\exp^{-j\frac{\Omega L}{2}}.sin(\frac{\Omega L}{2}) \tag{4.5}$$

where $\Omega L = \Omega_x L_x + \Omega_y L_y$

Thus blurring operator is known when the displacements are estimated correctly. So once we are able to estimate motion from our motion-smear model, we can restore original image as discussed above. Thus motion-smear model can be used as image restoration method.

Chapter 5

Simultaneous Estimation of Motion and Depth

5.1 Brief Introduction

Determination of object distance from defocused images has been investigated by many researchers. It has been found that the defocus operator contains the depth information, so it can be exploited to estimate the distance of an object. Using the same idea we have incorporated the defocus information in our motion-smear model to estimate depth and motion parameters simultaneously. In the following section a brief concept of depth from defocus (i.e, how defocus information helps us to obtain the distance of an object) has been introduced. Then we try to incorporate the defocus information in our motion-smear model. For this a new data acquisition strategy has been introduced which helps to get a system model which contains both the motion and depth information.

5.1.1 Depth from Defocus

Fig. 5.1 illustrates the image formation in a simple camera. Let P be a point on a visible surface in the scene and p be its focused image. P and p is related by the well known lens formula as

$$\frac{1}{f} = \frac{1}{u} + \frac{1}{v} \tag{5.1}$$

where u is the object distance and v is the image distance. If P is not in focus it gives rise to a blurred image. According to geometric optics, the blurred image of P has the

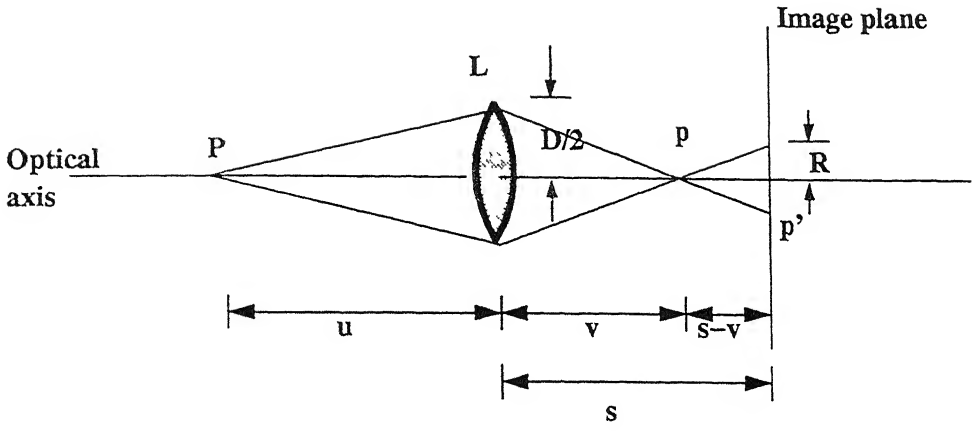

Figure 5.1: Image formation in a simple camera system

same shape as the lens aperture but scaled by a factor. Let the blurred image of the point P be $h(x, y)$. This $h(x, y)$ is known as the point spread function. If we consider camera systems having a circular aperture, then the blurred image of a point on the image detector is circular in shape and is called the *blur circle*. Let R be the radius of the blur circle and D be the diameter of the lens aperture, and s be the distance from the lens to the image detector plane. From the geometry it can be shown that

$$R = s\frac{D}{2}\left[\frac{1}{f} - \frac{1}{u} - \frac{1}{s}\right] \tag{5.2}$$

According to geometric optics, the intensity within the blur circle is approximately constant. If we further assume the camera to be a lossless system we get

$$h(x, y) = \begin{cases} \frac{1}{\pi R^2} & \text{if } x^2 + y^2 \leq R^2 \\ 0 & \text{otherwise} \end{cases} \tag{5.3}$$

where $h(x, y)$ is the PSF of the camera.Taking diffraction and non-idealities of lenses into account, an alternative model has been suggested for the intensity distribution given by two dimensional Gaussian function

$$h(x, y; \sigma) = \frac{1}{2\pi\sigma^2} e^{-\frac{1}{2}\frac{x^2+y^2}{\sigma^2}} \tag{5.4}$$

where σ is the spread parameter such that $\sigma = kR$ for $k > 0$. k is a constant of

proportionality characteristic of the given camera and mostly taken as $\frac{1}{\sqrt{2}}$[6].

If the radius R is a constant over some region on the image plane, the camera acts as linear shift invariant system. Therefore the observed defocused image $g_d(x,y)$ is the result of convolving the corresponding focused image $f(x,y)$ with camera's point spread function $h(x,y;\sigma)$, i.e,

$$g_d(x,y) = h(x,y;\sigma) \star f(x,y)$$

The point spread functions defined above are only two specific examples, it can be of other form which is characterized by the spread parameter σ which is the standard deviation of the distribution of any function h. For the circular point spread function spread is given by $\sigma = \frac{R}{\sqrt{2}}$. Hence once we know the spread σ of the defocus operator $h(x,y;\sigma)$ we can easily find out the depth using equation (5.2) which shows that the spread linearly depends on the inverse distance u^{-1}.

5.2 A General Definition for the Spread Parameter

The form of the spread function determines the definition of spread. This is generally assumed to be one of the point spread functions as defined in (5.3) or (5.4). However in practical optical systems, due to diffraction effects, aberrations etc., the effective point spread function can become quite complicated. Usage of circular or Gaussian function may result in inferior depth estimates because the definition of spread is intimately related to their form. If the point spread function of the optical system happens to be different because of other effects, then the estimate of spread is bound to get affected. Measuring the PSF from the camera itself, though, in general provides better results, but it is quite complicated and experiments have to be conducted with care. Therefore it would be desirable to have the definition of the spread independent of the form of the point spread function.

Def. : Let $h(x,y;\sigma)$ be any general defocus operator. We then define the normalized spread parameter as its second moment given by

$$\sigma^2 = \frac{1}{A_h} \int_{-\infty}^{\infty} \int_{-\infty}^{\infty} \left[(x-\overline{x})^2 + (y-\overline{y})^2 \right] h(x,y;\sigma) dx dy \tag{5.5}$$

where $(\overline{x},\overline{y})$ is the location of the center of mass of $h(x,y;\sigma)$ defined by

$$\begin{aligned} x &= \frac{1}{A_h} \int_{-\infty}^{\infty}\int_{-\infty}^{\infty} xh(x,y;\sigma)dxdy \\ y &= \frac{1}{A_h} \int_{-\infty}^{\infty}\int_{-\infty}^{\infty} yh(x,y;\sigma)dxdy \end{aligned} \tag{5.6}$$

and

$$A_h = \int_{-\infty}^{\infty}\int_{-\infty}^{\infty} h(x,y;\sigma)dxdy \tag{5.7}$$

In any practical optical system, the above defocus operator has the following properties:

- The defocus operator is rotationally symmetric.
- Assuming the camera to be lossless system

$$A_h = \int_{-\infty}^{\infty}\int_{-\infty}^{\infty} h(x,y;\sigma)dxdy = 1 \tag{5.8}$$

Even though the camera's aperture is not circular the spread of the defocus operator is linearly related to u^{-1}[6]. Hence, once we are able to estimate spread of the defocus operator by any means then the distance of object is easily found out.

5.3 A New Data Acquisition System

We take two successive frames $g_{01}(x,y;t_0,\Delta t_{01})$ and $g_{12_d}(x,y;\sigma_1;t_1,\Delta t_{12})$ by an imaging system with a non instantaneous shutter mechanism. The first frame is focused but it undergoes motion-smear during the exposure duration Δt_{01} of the imaging system. While during acquisition of the second frame, defocus is introduced deliberately so that the second frame gets defocused as well as motion smeared. Note that both the frames are taken in continuation. We then create a sum signal $s_{02_d}(x,y;\sigma_2;t_0,\Delta t_{02})$ from these two frames. Fig. 5.2 illustrates the method of acquiring two successive frames.

5.4 Mathematical Formulation of the Problem

Let $g_{01}(x,y)$ and $g_{12_d}(x,y)$ be two successive frames acquired as mentioned above (note that the time and spread dependence notation has been dropped for convenience) . If $f_0(x,y)$ is the original image then for linear space invariant system we have

$$\begin{aligned} x &= \frac{1}{A_h} \int_{-\infty}^{\infty}\int_{-\infty}^{\infty} xh(x,y;\sigma)dxdy \\ \bar{y} &= \frac{1}{A_h} \int_{-\infty}^{\infty}\int_{-\infty}^{\infty} yh(x,y;\sigma)dxdy \end{aligned} \tag{5.6}$$

and

$$A_h = \int_{-\infty}^{\infty}\int_{-\infty}^{\infty} h(x,y;\sigma)dxdy \tag{5.7}$$

In any practical optical system, the above defocus operator has the following properties:

- The defocus operator is rotationally symmetric.
- Assuming the camera to be lossless system

$$A_h = \int_{-\infty}^{\infty}\int_{-\infty}^{\infty} h(x,y;\sigma)dxdy = 1 \tag{5.8}$$

Even though the camera's aperture is not circular the spread of the defocus operator is linearly related to u^{-1}[6]. Hence, once we are able to estimate spread of the defocus operator by any means then the distance of object is easily found out.

5.3 A New Data Acquisition System

We take two successive frames $g_{01}(x,y;t_0,\Delta t_{01})$ and $g_{12_d}(x,y;\sigma_1;t_1,\Delta t_{12})$ by an imaging system with a non instantaneous shutter mechanism. The first frame is focused but it undergoes motion-smear during the exposure duration Δt_{01} of the imaging system. While during acquisition of the second frame, defocus is introduced deliberately so that the second frame gets defocused as well as motion smeared. Note that both the frames are taken in continuation. We then create a sum signal $s_{02_d}(x,y;\sigma_2;t_0,\Delta t_{02})$ from these two frames. Fig. 5.2 illustrates the method of acquiring two successive frames.

5.4 Mathematical Formulation of the Problem

Let $g_{01}(x,y)$ and $g_{12_d}(x,y)$ be two successive frames acquired as mentioned above (note that the time and spread dependence notation has been dropped for convenience) . If $f_0(x,y)$ is the original image then for linear space invariant system we have

$$\bar{x} = \frac{1}{A_h} \int_{-\infty}^{\infty}\int_{-\infty}^{\infty} xh(x,y;\sigma)dxdy$$
$$\bar{y} = \frac{1}{A_h} \int_{-\infty}^{\infty}\int_{-\infty}^{\infty} yh(x,y;\sigma)dxdy \tag{5.6}$$

and

$$A_h = \int_{-\infty}^{\infty}\int_{-\infty}^{\infty} h(x,y;\sigma)dxdy \tag{5.7}$$

In any practical optical system, the above defocus operator has the following properties:

- The defocus operator is rotationally symmetric.
- Assuming the camera to be lossless system

$$A_h = \int_{-\infty}^{\infty}\int_{-\infty}^{\infty} h(x,y;\sigma)dxdy = 1 \tag{5.8}$$

Even though the camera's aperture is not circular the spread of the defocus operator is linearly related to u^{-1}[6]. Hence, once we are able to estimate spread of the defocus operator by any means then the distance of object is easily found out.

5.3 A New Data Acquisition System

We take two successive frames $g_{01}(x,y;t_0,\Delta t_{01})$ and $g_{12_d}(x,y;\sigma_1;t_1,\Delta t_{12})$ by an imaging system with a non instantaneous shutter mechanism. The first frame is focused but it undergoes motion-smear during the exposure duration Δt_{01} of the imaging system. While during acquisition of the second frame, defocus is introduced deliberately so that the second frame gets defocused as well as motion smeared. Note that both the frames are taken in continuation. We then create a sum signal $s_{02_d}(x,y;\sigma_2;t_0,\Delta t_{02})$ from these two frames. Fig. 5.2 illustrates the method of acquiring two successive frames.

5.4 Mathematical Formulation of the Problem

Let $g_{01}(x,y)$ and $g_{12_d}(x,y)$ be two successive frames acquired as mentioned above (note that the time and spread dependence notation has been dropped for convenience) . If $f_0(x,y)$ is the original image then for linear space invariant system we have

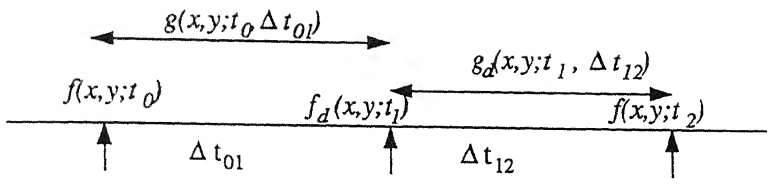

here $f_d(x,y;t_1)=f_1(x,y;t_1) * h_d(x,y)$;

Figure 5.2: Graphical description of data acquisition

$$g_{01}(x,y) = f_0(x,y) \star h_{01}(x,y;\mathbf{v}) \tag{5.9}$$
$$g_{12_d}(x,y) = f_{1_d}(x,y) \star h_{12}(x,y;\mathbf{v}) \tag{5.10}$$

where $h_{01}(x,y;\mathbf{v})$, $h_{12}(x,y;\mathbf{v})$ are the motion smearing operator as explained in the previous chapter. Further, in the space-invariant case $f_{1_d}(x,y)$ can be written as

$$f_{1_d}(x,y) = f_1(x,y) \star h_d(x,y;\sigma) \quad \text{and} \tag{5.11}$$
$$f_1(x,y) = f_0(x,y) \star \delta(x - L_x, y - L_y); \text{ with } L_x = v_x \Delta t_{01}, L_y = v_y \Delta t_{01} \tag{5.12}$$

From (5.12) $f_{1_d}(x,y)$ can be rewritten as

$$f_{1_d}(x,y) = f_0(x,y) \star h'(x,y) \star h_d(x,y;\sigma); \tag{5.13}$$
$$\text{with } h'(x,y) = \delta(x - L_x, y - L_y)$$

If we create a sum signal by adding the two frames as

$$s_{02_d}(x,y) = g_{01}(x,y) + g_{12_d}(x,y)$$

then from (5.9), (5.10) and (5.13) we have

$$\begin{aligned} s_{02_d}(x,y) &= g_{01}(x,y) + g_{12_d}(x,y) \\ &= f_0(x,y) \star h_{01}(x,y;\mathbf{v}) + f_0(x,y) \star h'(x,y) \star h_d(x,y;\sigma) \star h_{12}(x,y;\mathbf{v}); \\ &= f_0(x,y) \star (h_{01}(x,y;\mathbf{v}) + h'(x,y) \star h_d(x,y;\sigma) \star h_{12}(x,y;\mathbf{v})) \end{aligned} \tag{5.14}$$

In discrete domain, (5.9) and (5.14) can be expressed as

$$\begin{aligned} g_{01}(k,l) &= f_0(k,l) \star h_{01}(k,l) \\ s_{02_d}(k,l) &= f_0(k,l) \star h_{02_d}(k,l) \qquad (5.15) \\ \text{where } h_{02_d}(k,l) &= h_{01}(k,l) + h'(k,l) \star h_d(k,l;\sigma) \star h_{12}(k,l) \qquad (5.16) \end{aligned}$$

In frequency domain, we have from (5.16)

$$\begin{aligned} G_{01}(\omega_1,\omega_2) &= F_0(\omega_1,\omega_2)H(\omega_1,\omega_2) \text{ and} \\ S_{02_d}(\omega_1,\omega_2) &= F_0(\omega_1,\omega_2)(H_{01}(\omega_1,\omega_2) + H'(\omega_1,\omega_2)H_d(\omega_1,\omega_2)H_{12}(\omega_1,\omega_2)) \end{aligned} \qquad (5.17)$$

Since the two exposure durations Δt_{01} and Δt_{12} are same, we have

$$H_{01}(\omega_1,\omega_2) = H_{12}(\omega_1,\omega_2) \qquad (5.18)$$

From (5.17) and (5.18) we have

$$\begin{aligned} S_{02_d}(\omega_1,\omega_2) &= F_0(\omega_1,\omega_2)H_{01}(\omega_1,\omega_2)(1 + H'(\omega_1,\omega_2)H_d(\omega_1,\omega_2)) \\ &= G_{01}(\omega_1,\omega_2)(1 + H'(\omega_1,\omega_2)H_d(\omega_1,\omega_2)) \\ \text{or } S_{02_d}(\omega_1,\omega_2) &= G_{01}(\omega_1,\omega_2)H(\omega_1,\omega_2); \qquad (5.19) \end{aligned}$$

where $H(\omega_1,\omega_2) = 1 + H'(\omega_1,\omega_2)H_d(\omega_1,\omega_2)$

Here $H'(\omega_1,\omega_2)$ is given as

$$H'(\omega_1,\omega_2) = FT\{h'(k,l)\} = \exp(-j\omega L); \qquad (5.20)$$

where $\omega L = \omega_1 L_x + \omega_2 L_y$

Equation (5.19) can be written in spatial domain as

$$s_{02_d}(k,l) = g_{01}(k,l) \star h(k,l) \qquad (5.21)$$

where

$$h(k,l) = \delta(k,l) + h'(k,l) \star h_d(k,l) \qquad (5.22)$$

Fig. 5.3 illustrates the equation (5.21). Now the problem reduces to system identification problem in which we have to estimate $H(z_1,z_2)$ from the input-output data. As

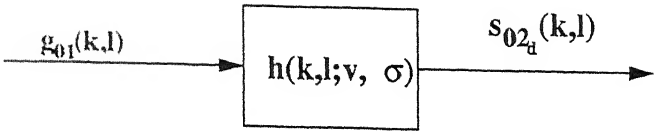

Figure 5.3: Representation of the underlying system.

explained in chapter 3 we can approximate $H(z_1, z_2)$ by polynomial transfer function using *Equation error identification algorithm.*

5.5 Estimation of Depth and Displacement from the Approximated Transfer Function.

Once we are able to approximate $h(k,l)$, it is easy to find the spread and displacement. As we see from (5.22)

$$\begin{aligned} h(k,l) &= \delta(k,l) + h'(k,l) \star h_d(k,l) \\ \text{or, } h(k,l) - \delta(k,l) &= h'(k,l) \star h_d(k,l) \end{aligned} \tag{5.23}$$

Let

$$h_1(k,l) = h'(k,l) \star h_d(k,l) \tag{5.24}$$

Equation (5.24) has the same property as that of defocus operator $h_d(k,l;\sigma)$, except that it has the centroid shifted by (L_x, L_y). In other words, equation (5.24) represents a defocus operator with center of mass at (L_x, L_y). Hence the center of mass of $h_1(k,l)$ gives the displacements and its second moment gives the spread σ. Hence, once we have $h(k,l)$ we can easily find $h_1(k,l)$ by subtracting 1 from $h(0,0)$. The displacements and the spread can then be calculated from its first and second moment respectively as defined in equations (5.5) and (5.6).

Chapter 6

Experimental Results

The methods discussed in the previous chapters have been implemented to test their efficacy and accuracy. First, the results on motion estimation are discussed. We tested the motion-smear algorithm on simulated test pictures. Further, we restored the blurred image using the motion information as discussed in chapter 4. Finally, we tested our algorithm for simultaneous estimation of motion and depth.

6.1 Results on Simulated Smeared Image Frames

Referring to equation (2.1), we have,

$$\begin{aligned} g(x,y;t_i,\Delta t_{i,i+1}) &= \frac{1}{\Delta t_{i,i+1}} \int_{t_i}^{t_{i+1}} f(x,y;t) l(t;t_i,\Delta t_{i,i+1}) dt \\ &= \frac{1}{T} \sum_{k=0}^{T-1} f(x,y;t^{(k)}) l(t^{(k)};t_i,\Delta t_{i,i+1}) \end{aligned}$$

where the interval $(t_i, t_{i+1}]$ is divided into T time steps. It means we can simulate $g(x,y)$ by summing up unblurred images obtained at incrementally different camera translations corresponding to camera positions at instants $t^{(k)}$. We adopted two methods to obtain two successive frames of motion smeared images. In the first method we take an image of size $N \times N$ of which only the region $N_1 \times N_1$ ($N_1 < N$) is considered to avoid the boundary problems. From the $N \times N$ image, we created successive frames such that each frame is shifted by some pixels (say 1) w.r.t its previous frame in the x-direction. Then the two required smeared frames g_{01} and g_{12} are obtained by adding the frames as discussed above. In a similar way motion-smear along both the x and y

directions can be created.

Figures 6.1, 6.3 and 6.5 show the results obtained during the testing of motion-smear algorithm on the test images simulated as discussed above. We selected a local region of size 41×41 assuming the maximum displacements to be 10 pixels in either directions. We then selected the order of the filter as discussed in chapter 3. Three cases have been considered. Fig. 6.1 shows the result of a cameraman image which is motion smeared by 5-pixels displacements along positive x-direction. In Fig. 6.3 the cameraman image is smeared by 6-pixels displacements along both the direction. Fig. 6.5 shows the motion smeared images with $L_x = 6$ and $L_y = 3$. In each of the cases the PSF, optical flow and the plot of MSE vs. the value of M have been shown. As we see from the mesh plot of the PSF, there are two impulses, one at the origin and the other one at (L_x, L_y) . Figs. 6.2 , 6.4 and 6.6 show the restored images using the regularized inverse filter with different values of γ for each of the cases discussed above.

Results for the noisy frames with SNR=25dB are shown in the fig. 6.7. Figs. 6.7(a) and 6.7(b) are the two noisy motion-smeared frames with $L_x = 5$ and $L_y = 0$. We have estimated the PSF for both the cases (i.e, when both the input and output signals are denoised and when only input image is denoised). Figs. 6.7(c) and 6.7(d) show the PSFs for the two cases respectively. Fig. 6.7(e) shows the PSF estimated for the brick image with $L_x = 5$ and $L_y = 5$ under noisy condition (SNR=25dB). The size of the local region is taken as 51×51. We have used Gaussian filter of size 3×3 and variance 0.5 for denosing the signal. The value of displacements calculated as first moment of the PSF are shown in the figure itself. Figs. 6.7(g), 6.7(h) and 6.7(i) show the estimated optical flow for the three cases as mentioned above. The test image taken here is highly textured. The performance of the motion estimation algorithm on noisy textured image is better than that of noisy cameraman image.

In the second method of data simulation, a shot of 1 second was taken from the digital camera connected to frame grabber board. In the shot, the person is holding a box which he moves slowly to his right during the shot with no body movement. This shot contains a sequence of 7 frames. The first three frames were added to create first frame g_{01} and the next three added to create g_{12}. Fig. 6.8 shows the results of motion estimation algorithm using the test images created by the shot of 1 second. The local area of size 51×51 was taken with $M = 5$ for estimating the displacements. Two PSF has been shown in this result. One is for the area where there is no movement and the other is for the area containing the box. L_x and L_y calculated by analytical expression varies from $L_x = -1.2$ to -1.8 and $L_y = 0.23$ to 0.45 over the area containing the

box and nearly zero at other parts. Fig. 6.8(d) shows the estimated optical flow over some points of the image. The optical flow clearly shows some motion along negative x-direction near box area.

Figs. 6.9 and 6.10 show the results for the algorithm developed to estimate motion and depth simultaneously. In this case two successive frames of smeared images g_{01} and g_{12_d} are created. Motion smear is simulated by the first method as discussed earlier. For defocus we have used the pill box function with radius $R = 3$. The local region of size 53×53 is used for estimating the parameters assuming a maximum displacement of 10-pixels in either directions and a maximum blur circle of radius 3-pixels. Fig. 6.9 shows the result for the test images which contain both motion smear and defocus blur. The first frame is focused and motion-smeared by 4-pixels displacements along positive x-direction and the second frame is defocused and motion smeared. The radius used here is $R = 3$ pixels. The optical flow and the spread map are shown in figs. 6.9(e) and 6.9(f). The mesh plot of PSF is shown in fig. 6.9(h) and the function $h_1(k, l)$ obtained from the PSF is plotted in fig.6.9(i). As we clearly see from the plot that there is a circle shifted away from the origin. The amount of shift gives us the value of displacements and the radius of the circle is the blur circle radius. We calculated the displacements and the spread as $L_x = 4.01$ $L_y = .012$ and $\sigma = 2.167$ analytically (as discussed in the chapter 5). These values are found to be close to their true values. In fig. 6.10 the bark image is motion smeared by 6-pixels along positive x and y direction. The amount of defocus used is same as in previous example. From the figure we note that the computed spread over the entire image is constant and very close to actual value (the calculated $\sigma = 2.165$).

The method discussed in [2] for estimating motion from motion-smear model uses exhaustive search method. It also uses a special sort of sensor arrangement to avoid instability problem. In our case we have considered a boxcar model. There is no problem in estimating stable PSF, as we are approximating the unknown transfer function by a polynomial transfer function. The algorithm proposed in [2] behaves good under noisy condition. In the present case, good denoising of the input signal is essential for better estimation of the PSF. Output noise doesn't affect the estimation of transfer function coefficients as seen in chapter 3. We have tested our algorithm on a noisy and smeared textured image and obtained good results. All of the existing methods for image motion estimation use displacement as a cue. Consequently, they all suffer from temporal aliasing[2]. There is no such problem of temporal aliasing in motion smear model.

To the best of our knowledge, simultaneous estimation of motion and depth from

smeared images has not been considered so far.

(a)

(b)

(c)

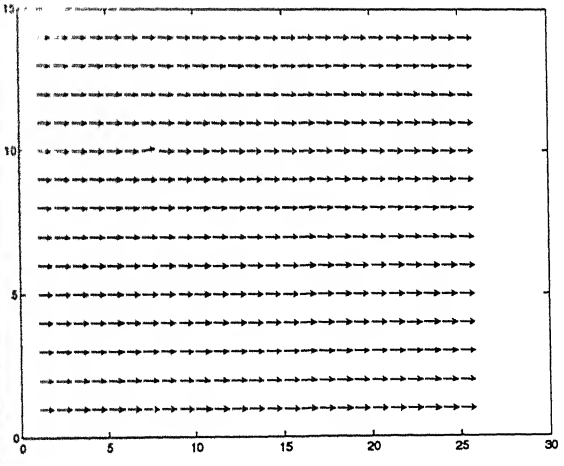

(d)

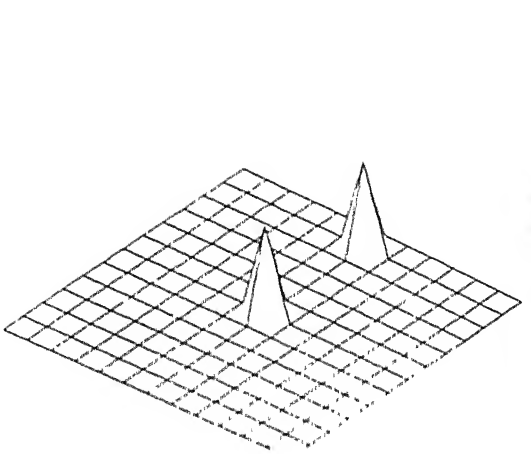

(e)

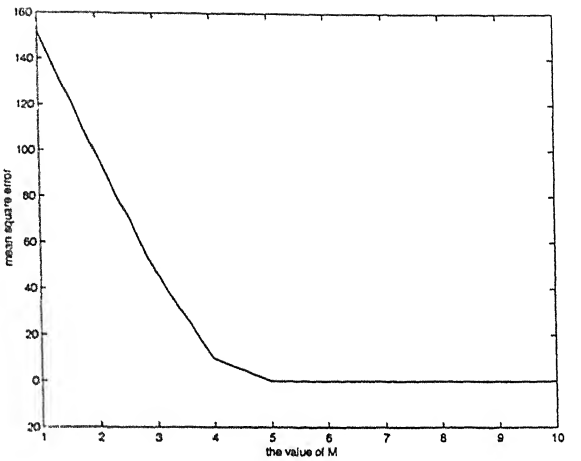

(f)

Figure 6.1: (a) The original image of cameraman (b) Image g_{01}, motion smeared by 5 pixels displacement along positive x-direction (c) More smeared image s_{02} (d) The estimated optical flow over a portion of the image (e) The PSF of a local region size (41×41) with $M = 6$ (e) Plot of mean square equation error vs. M

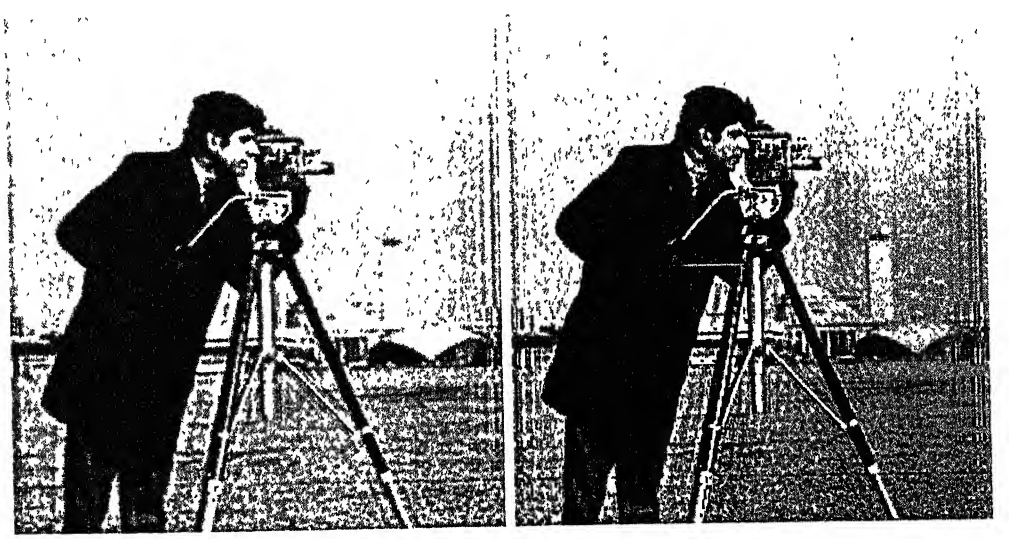

(a) (b)

Figure 6.2: Restored images with different value of gamma (a) $\gamma = .01$ (b)$\gamma = .001$

(a) (b)

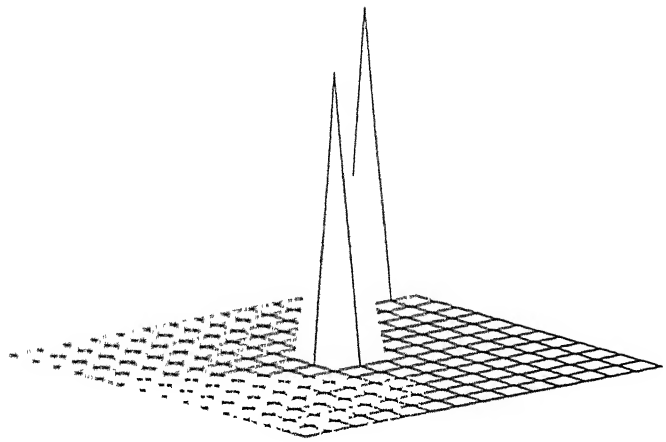

(c)

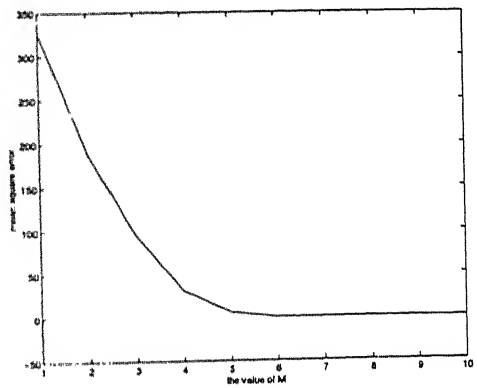

(d)

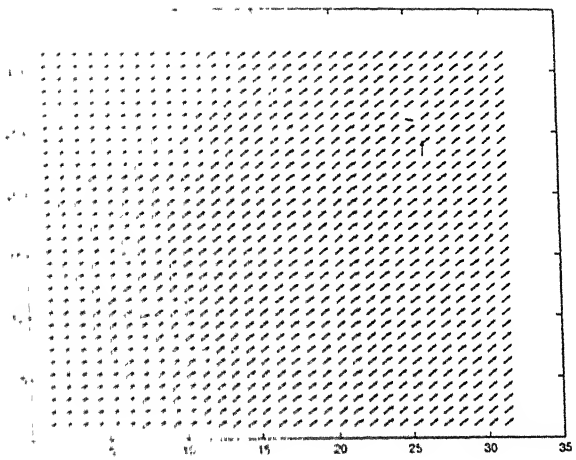

(e)

Figure 6.3: (a) Image g_{01}, motion smeared by 6 pixels displacement along positive x and y direction (b) The summed up signal (more smeared) (c) The PSF of a local region of size 41 × 41 with $M = 7$ (d) Plot of mean square equation error vs M (e) The estimated optical flow over some portion of the image.

(a) (b)

Figure 6.4: Restored images with different value of regularizing parameter γ (a) $\gamma = .01$ (b) $\gamma = .007$

(a) (b)

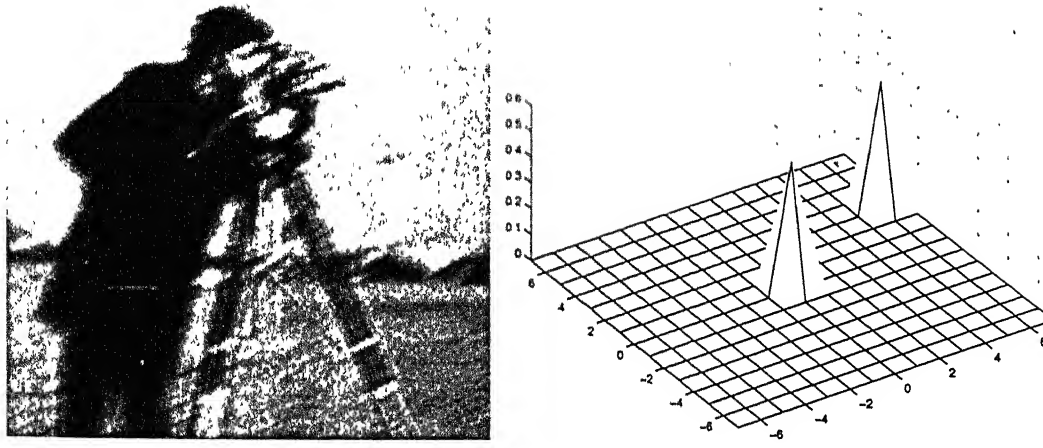

(c) (d)

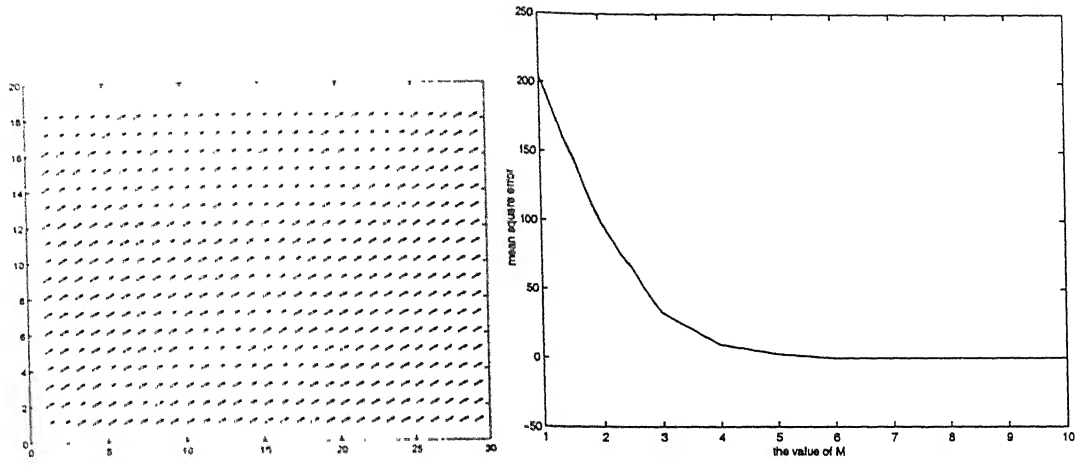

(e) (f)

Figure 6.5: (a) Image g_{01}, motion smeared with $L_x = 6, L_y = 3$ (b) Image g_{12} (c) The sum signal s_{02} (d) The PSF of a local region of size 41×41 with $M = 7$ (e) The estimated optical flow over some points of the image. (f) Plot of MSE vs. the value of M

(a) (b)

Figure 6.6: Restored images using regularized inverse filter with (a) $\gamma = .05$ (b) $\gamma = .025$

(a) (b)

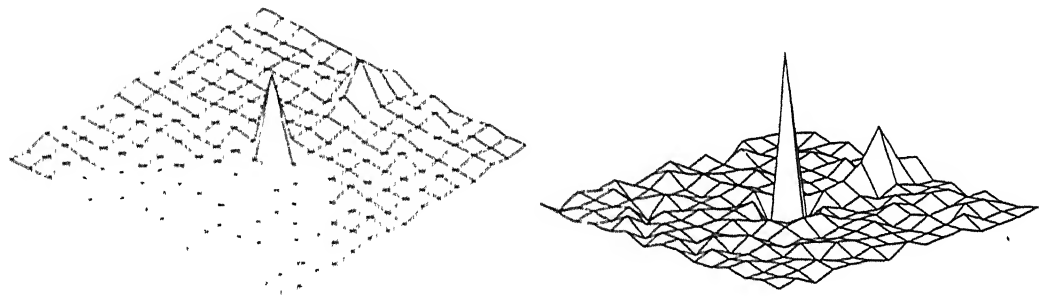

(c) (d)

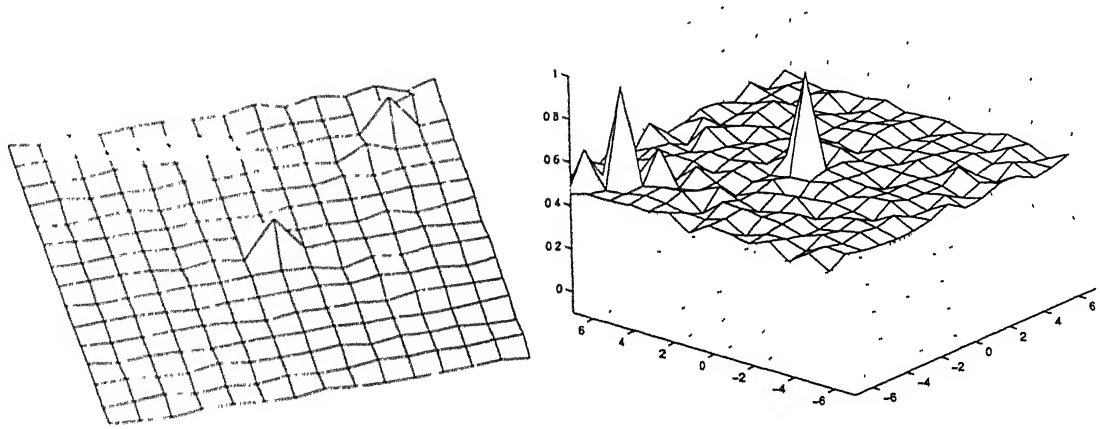

(e) (f)

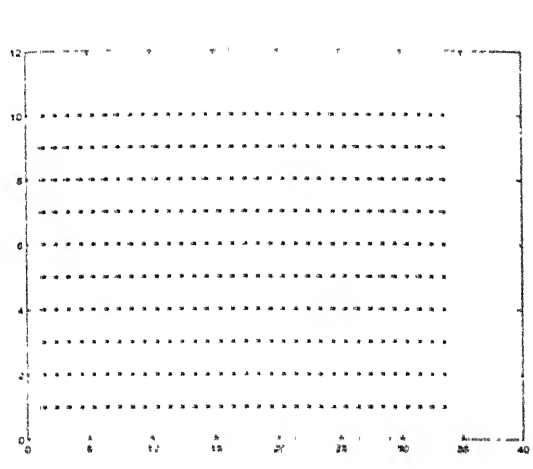

(g)

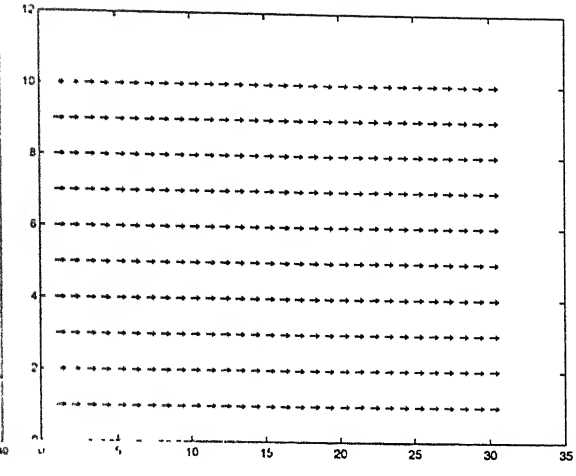

(h)

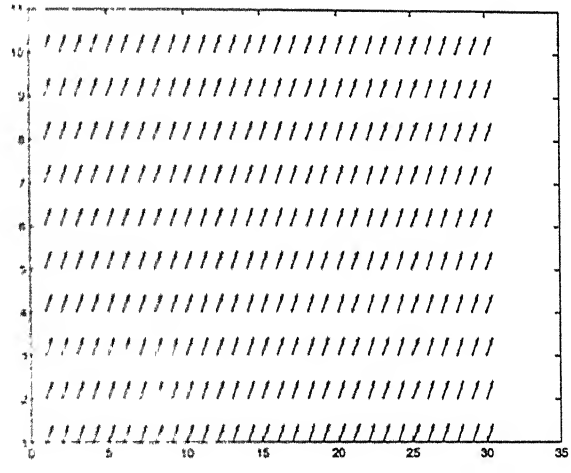

(i)

Estimated displacements in (c) $L_x = 4.98$ $L_y = .025$ (d) $L_x = 5.06$ $L_y = 0.016$ (e) $L_x = 4.879$ $L_y = 4.96$

Figure 6.7: Results for the noisy case. (a) Noisy image g_{01_n}, (b) Summed up signal s_{02_n} (c) PSF of the local region of size 51×51 with $M = 6$ and $L_x = 5$ $L_y = 0$ for the case when both the input and output signals are denoised. (d) PSF estimated when only input signal is denoised (e) Top view of the PSF of a local region with $L_x = L_y = 5$ (f) Side view of the PSF (g) The estimated optical flow over some regions of the image for the case when both the signals are denoised (h) Optical flow diagram when only input is denoised (i) Optical flow diagram for the images, motion smeared by 5-pixels displacements along positive x and y direction.

(a) (b)

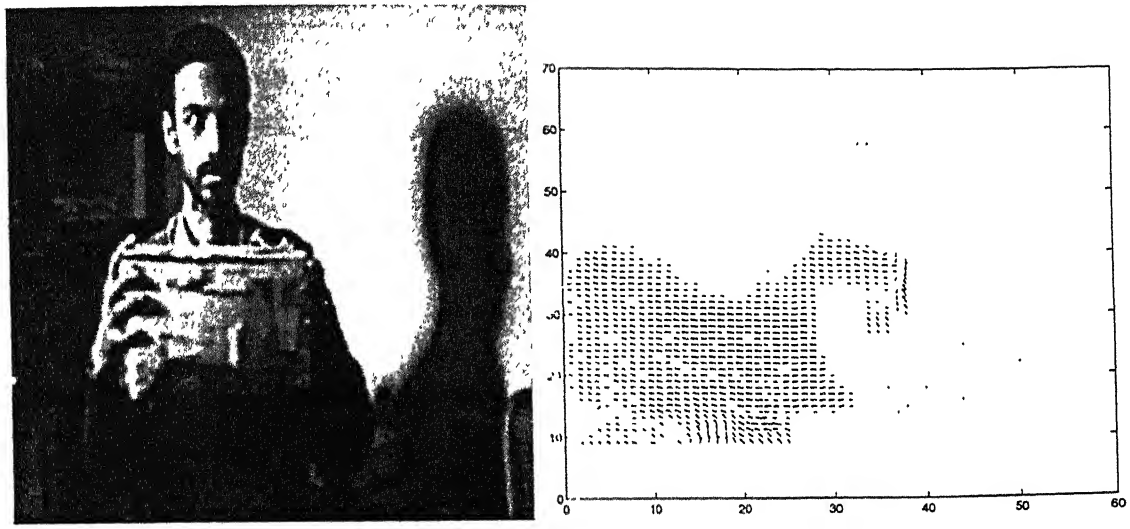

(c) (d)

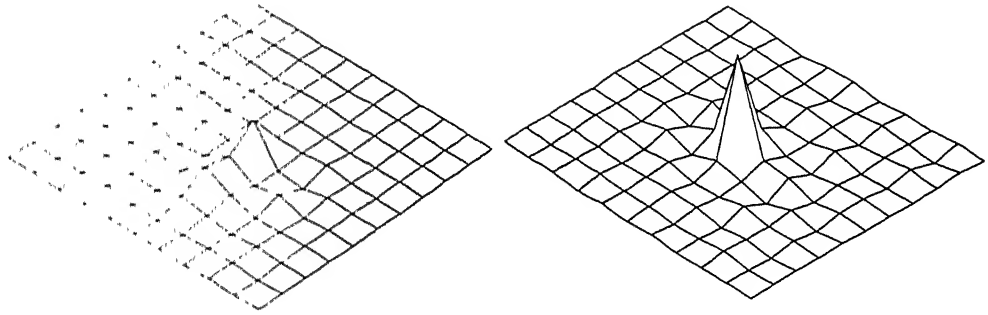

(e) (f)

Figure 6.8: (a) The original image of rajiv (b) Image g_{01}, motion smeared (c) More smeared image s_{02}(d) The estimated optical flow over a portion of the image (e) The PSF of the box area of size 41×41 with $M = 5$ (f) The PSF of the head area.

(a)

(b)

(c)

(d)

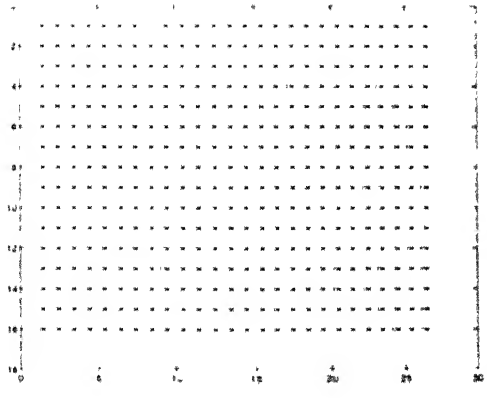

(e)

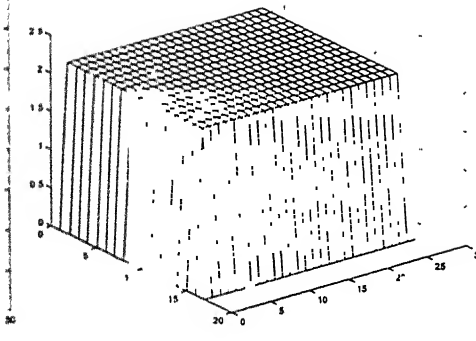

(f)

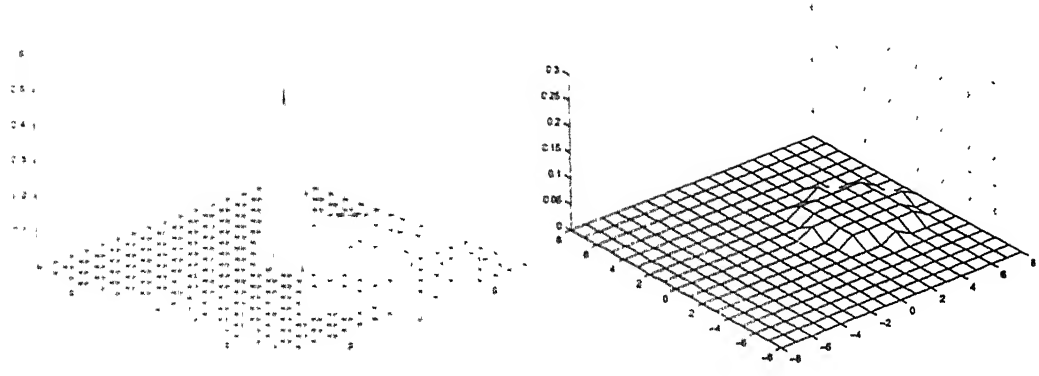

(g) (h)

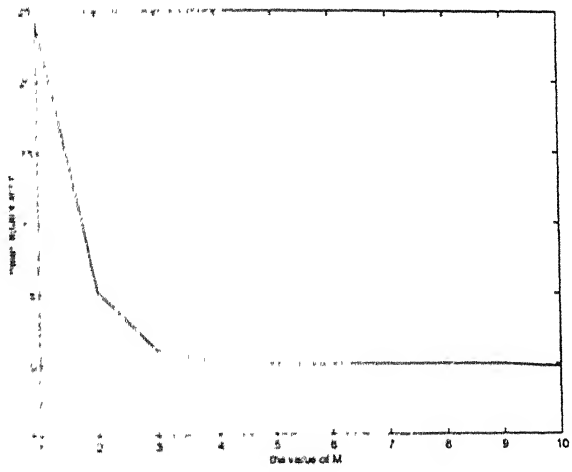

(i)

M	1	2	3	4	5	6	7	8	9	10
MSE	24.1897	5.2123	1.0570	.2017	.0194	.0005	.0000	.0000	.0000	.00000

Figure 6.9: (a) The original image of cameraman (b) Image g_{01}, motion smeared by 4 pixels displacements along x-direction. (c) Image g_{12_d}, defocused and motion smeared (d) The sum signal s_{02_d} (e) The estimated optical flow over some points of the image (f) The spread map (g) The PSF of a local region of size (53×53) with $M = 8$ (h) The function $h_1(k, l)$ (i) Plot of MSE vs. the value of M

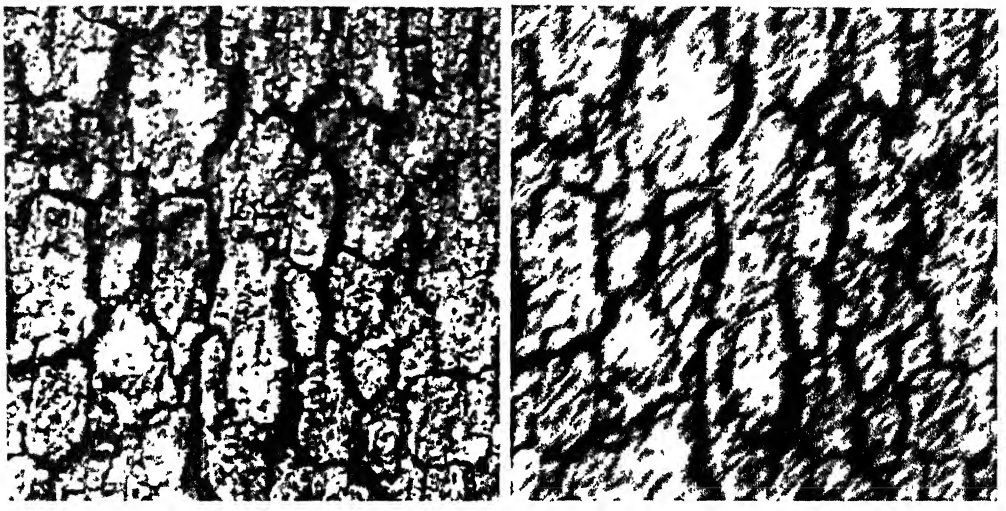

(a) (b)

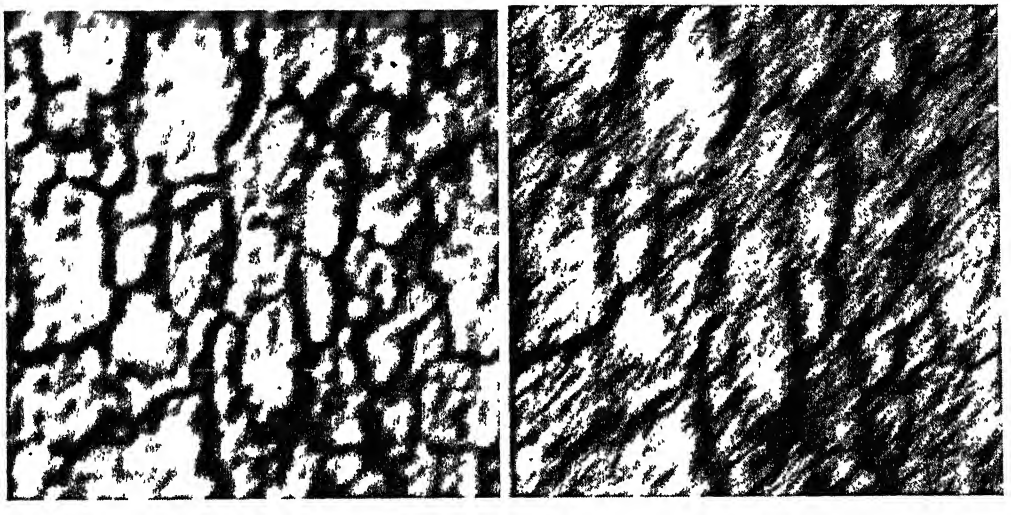

(c) (d)

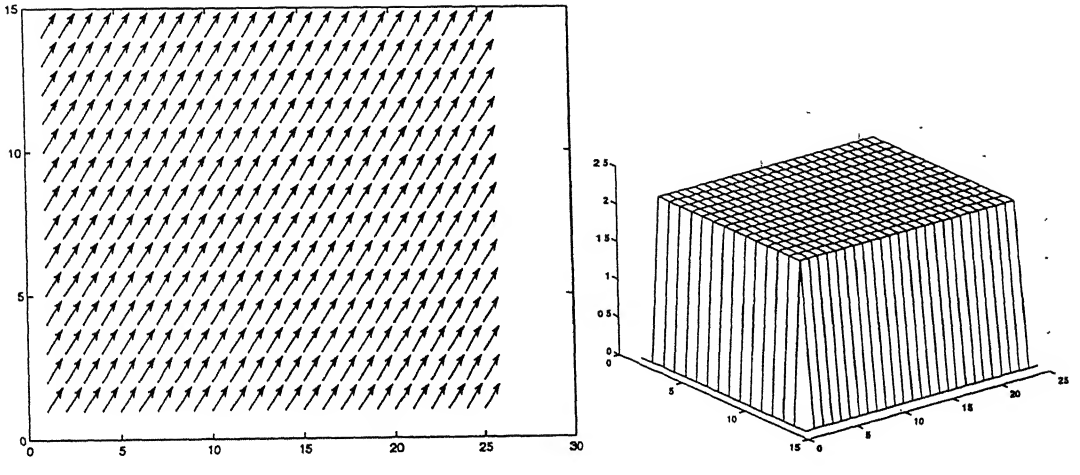

(e) (f)

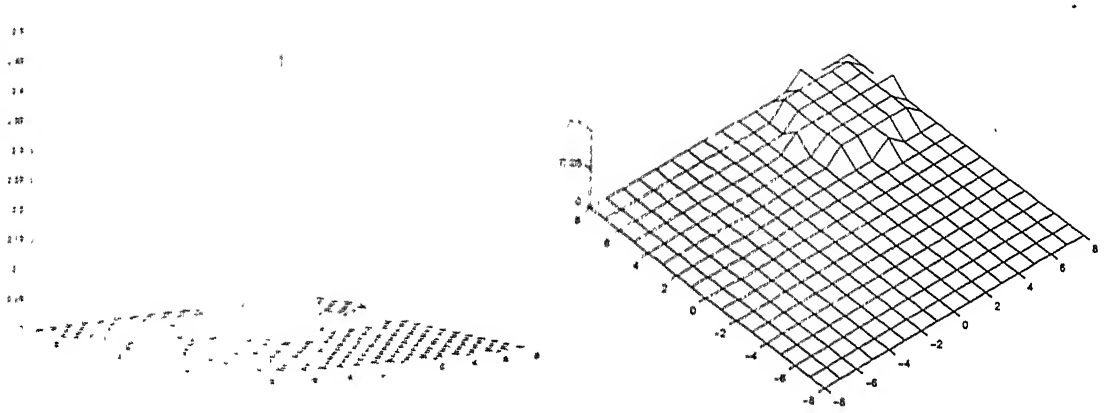

(h)

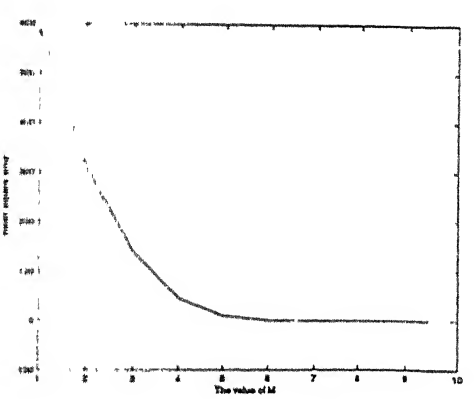

(i)

	1	2	3	4	5	6	7	8	9	10
error	591 6419	807 5076	138 3907	45.2994	10.1765	1.1191	.0276	.0000	.0000	.000

Figure 6.10: (a) The original image of bark texture (b) Image g_{01}, motion-smeared by 5 pixels displacements along both the direction (c) Image g_{12_d}, defocused as well as motion smeared (d) Sum signal s_{02_d} (e) The estimated optical flow over some points of the image (f) Spread map (g) The PSF $h(k,l)$ of a local region of size (53×53) with $M = 8$ (h) The function $h_1(k,l)$ (i) Plot of mean square equation error vs. the value of M.

Chapter 7

Conclusions and Scope for Future Work

We have proposed motion estimation from motion smeared images using the method of system identification. The motion estimated can also be used in image restoration by using [illegible] inverse filter. Further, the method can be reformulated to estimate motion and depth [illegible]. We see that motion-smear and defocus blur, which are considered as [illegible] in the image, can be exploited to yield two very vital parameters motion and depth. The simulation results show that the proposed method can estimate depth and motion correctly by proper selection of the window size and that of the order of the [illegible] polynomial. It is also observed that estimation of motion from smear is less sensitive to temporal aliasing when compared to methods based on [illegible] cues.

Motion and depth estimation from degradation is emerging area of research. Though a lot of work has been done in depth field using defocus concept, motion estimation from motion smear is a relatively new concept. The fusion of motion smear and defocus concept is really a very challenging work. New methods can be developed using multiframes or single frame.

Bibliography

[1] D. Burr, "Motion Smear, " *Nature*, Vol. 284, pp. 164-165, Mar. 1980.

[2] W.G. Chen, N. Nandhakumar, and W. Martin, "Image Motion Estimation From motion Smear - A New Computational Model ," *IEEE Trans. on Pattern Analysis and Machine Intelligence*, Vol. 18, N0. 4, April 1996.

[3] P.A. Regalia, *Adaptive IIR Filtering in Signal Processing and control*, Marcel Dekker, Inc. , 1995.

[4] J. D. Rayala, "*Estimation of Depth for Monocular Defocued Images", Ph.D Thesis*, Department of Electrical Engineering, Indian Institute of Technology, Kanpur, May 1997.

[5] Sqn Ldr Vinu Thomas, "Estimation of Motion from Motion Smeared Images," M.Tech thesis, Department of Electrical Engineering, Indian Institute of Technology, Kanpur, April 1998.

[6] M. Subbarao, "Determining Distance from Defocused Images of Simple Objects". Submitted to *IEEE Trans. on PAMI.*

[7] D. Slepian, "Restoration of Photographs Blurred by Image Motion," *The Bell System Technical Journal*, Dec. 1967.

[8] J. S. Lim, *2D Signal and Image Processing*, Prentice Hall, 1990.

[9] N. B. Karayiannis and A. N. Venetsanopoulos, "Regularising Theory in Image Restoration- The Stabilizing Functional Approach," *IEEE Trans. on ASSP*, Vol. 38, No. 7, July 1990.

[10] M. R. Banham and A. K. Katsaggelos, "Digital Image Restoration," *IEEE Signal Processing Magazine*, March 1997.

[11] J.S. Lee, "Digital Image Smoothing and the Sigma Filter, "*Computer Vision, Graphics, and Image Processing*, Vol. 24, pg. no. 255-269, 1983.

[12] Z. Myles and N.D. Vitoria Lobo, "Recovering Affine Motion and Defocus Blur Simultaneously ," *IEEE Trans on PAMI*, Vol. 20, No. 6, June 1998.

[13] R. C. Gonzalez and P. A. Wintz, *Digital Image Processing*, second edition, Addison-Wesley, 1987.

[14] H. C. Andrews and B. R. Hunt, *Digital Image Restoration*, Prentice-Hall, Englewood Cliffs, N.J., 1997.

[15] A.K. Jain, *Fundamentals in Digital Image Processing*, Prentice-Hall, Englewood Cliffs, N.J., 1989.

[16] The Oculus-F/64 Frame Grabber, User's Manual, Edition 1.0, Coreco Inc., Canada.

133667

Date Slip

The book is to be returned on the date last stamped.

.....	.....
.....	.....
.....	.....
.....	.....
.....	.....
.....	.....
.....	.....
.....	.....
.....	.....
.....	.....
.....	.....